THE JOURNAL OF PHYSICAL CHEMISTRY A

Article

pubs.acs.org/JPCA

Molecular Distances Determined with Resonant Vibrational Energy Transfers

Hailong Chen,† Xiewen Wen,† Jiebo Li, and Junrong Zheng*

Department of Chemistry, Rice University, 6100 Main Street, Houston, Texas 77005-1892, United States

Supporting Information

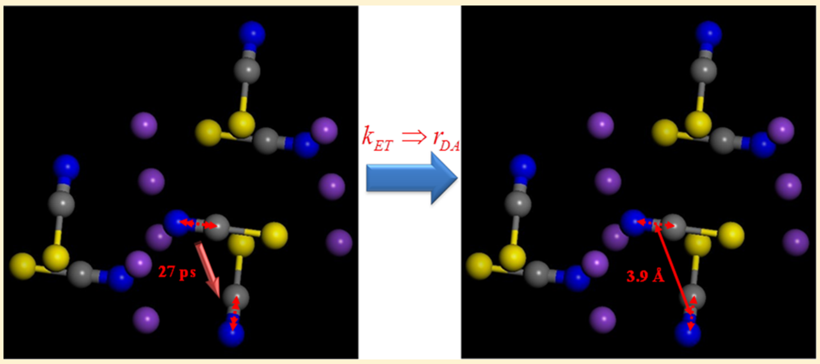

ABSTRACT: In general, intermolecular distances in condensed phases at the angstrom scale are difficult to measure. We were able to do so by using the vibrational energy transfer method, an ultrafast vibrational analogue of Förster resonance energy transfer. The distances among SCN^- anions in KSCN crystals and ion clusters of KSCN aqueous solutions were determined with the method. In the crystalline samples, the closest anion distance was determined to be 3.9 ± 0.3 Å, consistent with the XRD result. In the 1.8 and 1 M KSCN aqueous solutions, the anion distances in the ion clusters were determined to be 4.4 ± 0.4 Å. The clustered anion distances in aqueous solutions are very similar to the closest anion distance in the KSCN crystal but significantly shorter than the average anion distance (0.94−1.17 nm) in the aqueous solutions if ion clustering did not occur. The result suggests that ions in the strong electrolyte aqueous solutions can form clusters inside of which they have direct contact with each other.

1. INTRODUCTION

Short-ranged transient intermolecular interactions, for example, guest/host interactions, ion/ion interactions, and ion/molecule bindings, play significant roles in chemistry and biology. Electronic energy transfer methods, for example, Förster resonance energy transfer (FRET), are routinely applied to measure the distance between two molecules in many of these interactions.[1,2] In these methods, chromophores that can transfer and accept energy in the visible and near-IR frequency range are required to attach to molecules. The chromophores are typically at the size of 1−2 nm or larger, which is not only much larger than many of the intermolecular distances but also can perturb the molecular interactions under investigation. To probe molecular distances at the angstrom scale, what is needed is an ultrafast vibrational analogue of FRET of which the chromophores are simple chemical bonds (1−2 Å).

Here, by measuring ultrafast vibrational energy transfers in model systems of KSCN (potassium thiocyanate) crystals and aqueous solutions, we demonstrate that angstrom molecular distances in condensed phases can be determined. In this paper, we first present anisotropy decay and vibrational energy exchange data to show that vibrational energy can transfer resonantly among SCN^- anions and nonresonantly from SCN^- to $S^{13}C^{15}N^-$ with much slower rates in $KSCN/KS^{13}C^{15}N$ mixed crystals. A kinetic model is then developed to quantitatively analyze the resonant energy transfer data to obtain the resonant energy transfer time between two adjacent anions in the crystals. To convert the energy transfer time into distance, an equation based on the dephasing mechanism and the time-dependent Schrodinger equation is derived to correlate the energy transfer time with the energy donor/acceptor coupling strength, which is quantitatively correlated to the donor/acceptor distance under the dipole/dipole interaction. On the basis of the energy transfer equation and the dipole/dipole interaction equation and the measured energy transfer time, the distance between the two adjacent anions is calculated. The calculated distance is then compared to the distance measured by XRD. Within experimental uncertainty, the two values are the same. The uncertainty introduced by the point dipole assumption used in the method is then calculated based on the monopole theory. It is found that the uncertainty is very small, only ~1.3%, mainly because the donor/acceptor distance is more than three times larger than the sizes of the donor/acceptor. After benchmarking the vibrational energy transfer

Received: January 17, 2014
Revised: March 17, 2014
Published: March 18, 2014

method with the crystalline sample, the method is used to determine the anion distance in the ion clusters of KSCN aqueous solutions. It is found that within experimental uncertainty, the anion distance in the clusters is the same as that in the crystal.

2. EXPERIMENTS AND METHODS

2.1. Laser System. A ps amplifier and a fs amplifier are synchronized with the same seed pulse. The ps amplifier pumps an OPA to produce ~0.8 ps (vary from 0.7−0.9 ps in different frequencies) mid-IR pulses with a bandwidth of 10−35 cm^{-1} in a tunable frequency range from 400 to 4000 cm^{-1} with an energy of 1−40 μJ/pulse (1−10 μJ/pulse for 400−900 cm^{-1} and >10 μJ/pulse for higher frequencies) at 1 kHz. Light from the fs amplifier is used to generate a high-intensity mid-IR and terahertz supercontinuum pulse with a duration of <100 fs in the frequency range from <10 to >3500 cm^{-1} at 1 kHz. In nonlinear IR experiments, the ps IR pulse is the excitation beam (the excitation power is adjusted based on need, and the interaction spot varies from 100 to 500 μm). The supercontinuum pulse is the probe beam that is frequency-resolved by a spectrograph (the resolution is 1−3 cm^{-1}, dependent on the frequency), yielding the detection axis of a 2D IR spectrum. Two polarizers are added into the detection beam path to selectively measure the parallel or perpendicular polarized signal relative to the excitation beam.

2.2. Vibrational Energy Transfer Measurements. Vibrational lifetimes are obtained from the rotation-free 1−2 transition signal $P_{life} = P_{\parallel} + 2 \times P_{\perp}$, where $P_{\parallel}$ and $P_{\perp}$ are parallel and perpendicular data, respectively. The time-dependent anisotropy values are acquired from $r(t) = (P_{\parallel} - P_{\perp})/(P_{\parallel} + 2 \times P_{\perp})$, with the definition of time zero being a pump−probe delay of zero. The resonant energy transfer rate constants and the molecular rotational time constants in the samples are obtained from the anisotropy measurements. The isotropic distribution of a sample within the laser focus spot is tested by measuring the initial anisotropy values of the sample at different angles relative to the polarization of the excitation beam.

The nonresonant vibrational energy transfers among the regular KSCN and isotope-labeled $KS^{13}C^{15}N$ and $KS^{13}CN$ are measured with the vibrational energy exchange method.[3−5] In the measurements, the donor vibrational mode, for example, the CN (nitrile) stretch of KSCN is excited to its first vibrational excited state with an ultrafast IR pulse. The time-dependent decay of this CN first excited-state population is then monitored in real time with another laser pulse. Simultaneously, the first excited-state population of the acceptor mode, for example, the $^{13}C^{15}N$ stretch of $KS^{13}C^{15}N$, is also monitored in real time right after the donor is excited to its first excited state. Simultaneous analyses of the decay of the donor first excited-state population and the growth and decay of the acceptor first excited-state population according to the energy transfer kinetic model[3−5] quantitatively yield the vibrational energy transfer rate constant from the donor to the acceptor. Here, the vibrational mode that is excited by the laser is defined as the "donor". The mode that is not excited by laser but can accept energy from the donor is defined as the "acceptor". Experimentally, we can change the frequencies of the laser to selectively excite either the CN or $^{13}C^{15}N$ stretch so that both forward and backward energy transfers between these two stretches can be determined. The resonant energy transfers among the thiocyanate anions are measured with the resonant energy transfer induced anisotropy decay method.[4,6] In these measurements, the nitrile stretch of one anion, for example, SCN^-, is excited to its first excited state. The decay of the anisotropy value of this vibrational excitation signal is then monitored in real time. Simultaneous analyses on the anisotropy decays in samples with different mixed KSCN/$KS^{13}C^{15}N$ ratios quantitatively yield both the resonant energy transfer rate constant and the rotational time constant of the anion.

2.3. Samples. Unless specified, chemicals were purchased from Sigma−Aldrich and used without further purification. $KS^{13}C^{15}N$ was purchased from Cambridge Isotope Laboratory. The samples were thin films of polycrystalline KSCN/$KS^{13}C^{15}N$ mixed crystals with different molar ratios blended with ~50 wt % PMMA. The thickness of the sample is estimated to be a few hundred nm based on the CN stretch optical density. An optical image of a sample is provided in Figure S1 in the Supporting Information (SI). The function of PMMA was to suppress scattered light. The samples were placed in a vacuum chamber during measurements. There are four reasons to use KSCN and $KS^{13}C^{15}N$ and $KS^{13}CN$ as model systems: (1) the vibrational lifetimes of the nitrile stretches are relatively long (longer than 30 ps in D_2O solutions and even longer in the crystals as included in the SI);[4] (2) the transition dipole moments of the nitrile stretches are relatively large (0.3−0.4 D);[4] (3) the distance between any two anions in the KSCN crystal is well-characterized with XRD and neutron scattering, which can be used to benchmark the distance determined by the vibrational energy transfer method;[7] and (4) the phonon dispersion in the KSCN crystal was well-characterized before.[8,9]

The purpose of using different-isotope-labeled thiocyanate anion mixed samples, for example, a KSCN/$KS^{13}C^{15}N$ mixed crystal with different molar ratios, is 2-fold, (1) to shift the vibrational frequency of the nitrile stretch as the vibrational frequency of the CN stretch is different from that of the $^{13}C^{15}N$ stretch and (2) to change the number of resonant energy transfer acceptors in the samples without changing the crystalline structure or ion cluster structure because the isotope labeling has negligible effects on the intermolecular interaction between two thiocyanate anions that determines their distance and relative orientation.[10]

3. RESULTS AND DISCUSSION

3.1. Vibrational Energy Transferring among SCN^- Anions in the KSCN Crystal. Figure 1 displays the time-dependent normalized anisotropy values of the nitrile stretch (1st excited state) excitation of thiocyanate anion in two samples, (A) a 2% $KS^{13}C^{15}N$ in 98% KSCN ($KS^{12}C^{14}N$) mixed crystal (black) where $S^{13}C^{15}N^-$ is excited and (B) a pure KSCN crystal (red) where SCN^- is excited. In sample A, the anisotropy decays relatively slowly, with a single-exponential time constant of ~12 ps, and its residual anisotropy value at the delay time of 40 ps is ~50% of its initial value. In sample B, the anisotropy decays much faster, with a time constant ~1.8 ps. Its residual anisotropy value at 40 ps is only ~12% of the initial value. In general, the anisotropy decays have two possible molecular origins, (1) molecular reorientational motions and (2) energy transfers to molecules with different orientations. Both contribute to the orientational randomization of vibrational excitations and lead to the decay of signal anisotropy.[11] In the two samples, the crystalline structures and molecular interaction strengths are expected to be hardly changed by the isotope labeling with ^{13}C and ^{15}N on the anions because the

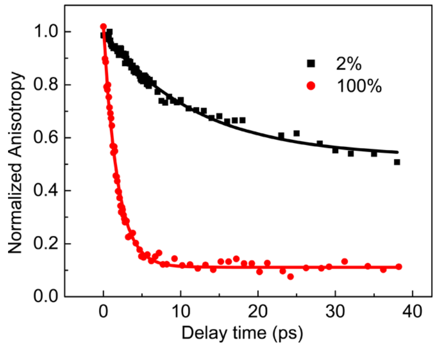

Figure 1. Time-dependent normalized anisotropy values of the nitrile stretch (1st excited state) excitation of the thiocyanate anion in two samples at room temperature: (A) a 2% $KS^{13}C^{15}N$ in 98% KSCN mixed crystal (black) where $S^{13}C^{15}N^-$ is excited and (B) a pure KSCN crystal (red) where SCN^- is excited. The decay of anisotropy indicates how fast the orientation of the vibrational excitation randomizes. Dots are data. Curves are single-exponential fits with time constants of 12 (sample A) and 1.8 ps (sample B). The 2 and 100% labels in represent the percentage of the resonant energy acceptors in the samples.

electronic structures of the atoms are expected to be little affected by the small changes of the atomic mass of the isotopes[10] and thus are essentially the same. Therefore, the anisotropy decays caused by molecular reorientational motions (wobbling) are very similar for the two samples. The observed large difference in anisotropy decay rate can only be caused by different energy transfer dynamics in the two samples.

In sample A, most of the neighbors of any excited $S^{13}C^{15}N^-$ are SCN^- ($S^{12}C^{14}N^-$). In sample B, all neighbors of the excited SCN^- are also SCN^-. The nitrile stretch energy transfer rate from a $S^{13}C^{15}N^-$ to a SCN^- is very different from the rate for energy transfer from one SCN^- to another SCN^-. As measured, the 0−1 transition frequency of the nitrile stretch of $S^{13}C^{15}N^-$ is 1975 cm^{-1}, 75 cm^{-1} smaller than that (2050 cm^{-1}) of SCN^-. The vibrational energy exchange rate between SCN^- and $S^{13}C^{15}N^-$ was directly measured using the vibrational energy exchange method.[4] From the 2D IR spectra shown in Figure 2, our vibrational energy exchange kinetic model,[3,4] and the principle of detailed balance, which requires that at equilibrium the populations at two energy levels fulfill the Boltzmann distribution, the energy transfer time constant ($1/k_{S^{13}C^{15}N^- \to SCN^-}$) from $S^{13}C^{15}N^-$ (1975 cm^{-1}) to SCN^- (2050 cm^{-1}) is determined to be 140 ± 7 ps in a $KSCN/KS^{13}C^{15}N$ = 1/1 mixed crystal. Details of this analysis are provided in the SI. This result indicates that the anisotropy decay caused by the two-stepped energy transfer from one $S^{13}C^{15}N^-$ to one SCN^- and from this SCN^- to another $S^{13}C^{15}N^-$ must be slower than 236 ps (the sum of the energy transfer times of the two-step energy transfer processes: $140 + 140 \times e^{-75/200} = 236$ ps) in sample A. This value is significantly longer than the measured anisotropy decay constant of 12 ps in sample A, indicating that the contribution of nonresonant energy exchanges between $S^{13}C^{15}N^-$ and SCN^- to the experimentally measured total anisotropy decay in sample A is negligible on this time scale. The contribution from resonant energy transfers among $S^{13}C^{15}N^-$ is also very small because the number of resonant energy acceptors in sample A is only 1/50 of that in sample B, which implies that the resonant energy transfer time in sample A should not be faster than 90 ps (1.8 × 50 = 90 ps) as the total energy transfer rate is linearly proportional to the total number

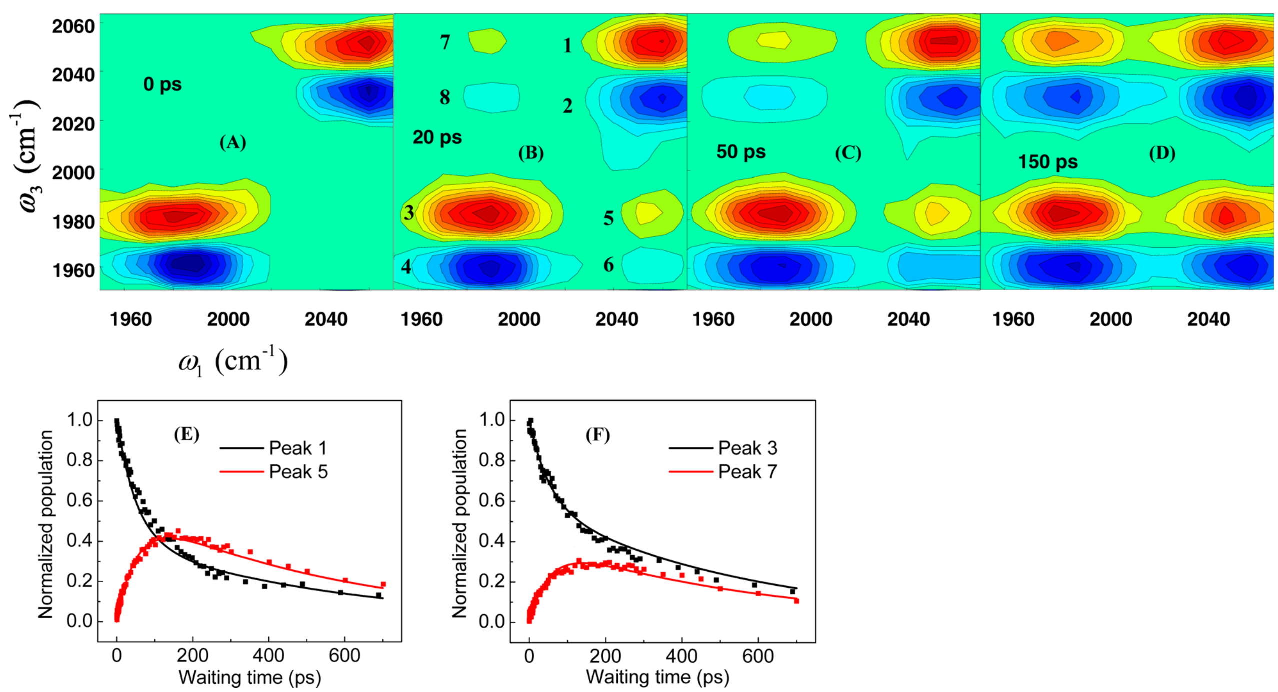

Figure 2. (A−D) Delay-time-dependent vibrational energy exchange 2D IR spectra of a $KSCN/KS^{13}C^{15}N$ = 1/1 mixed crystal at room temperature. The growth of cross peaks 5−8 indicates how fast the vibrational energy exchange proceeds between SCN^- and $S^{13}C^{15}N^-$. (E,F) Delay-time-dependent normalized intensities of peaks 1, 3, 5, and 7. Dots are experimental data, and curves are calculations based on the energy exchange kinetic model and experimentally measured vibrational lifetimes. Peaks 1 and 2 are the 0−1 and 1−2 transitions of the CN stretch, respectively, generated from direct laser excitation. Peaks 3 and 4 are the 0−1 and 1−2 transitions of the $^{13}C^{15}N$ stretch, respectively, generated from direct laser excitation. Peaks 5 and 6 are the 0−1 and 1−2 transitions of the $^{13}C^{15}N$ stretch, generated from the energy transfer process from CN to $^{13}C^{15}N$. Peaks 7 and 8 are the 0−1 and 1−2 transitions of the CN stretch, generated from the energy transfer process from $^{13}C^{15}N$ to CN.

dx.doi.org/10.1021/jp500586h | J. Phys. Chem. A 2014, 118, 2463−2469

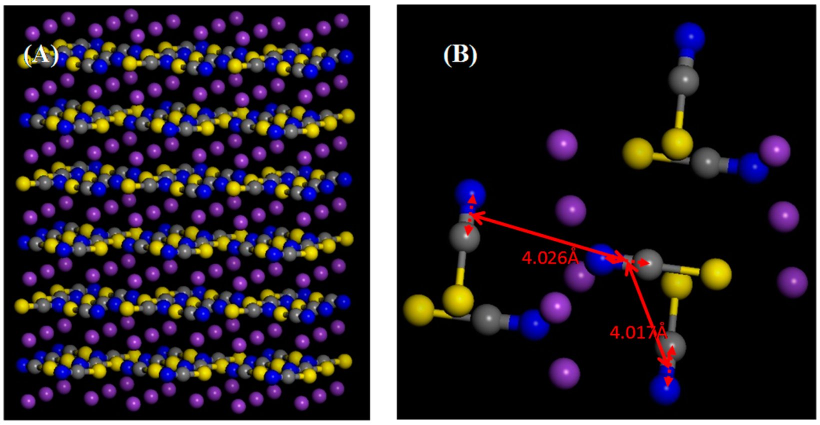

Figure 3. Crystalline structure of the KSCN crystal at room temperature. K is represented by purple balls, yellow balls for S, gray balls for C, and blue balls for N.

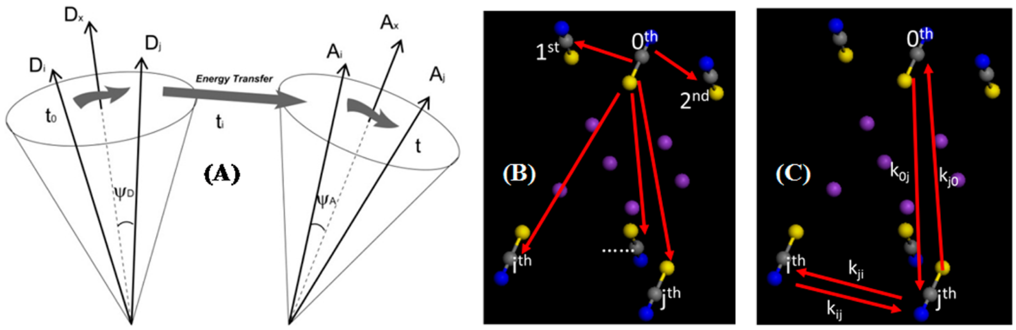

Figure 4. (A) Illustration of molecular wobbling and vibrational energy transfer from the donor (D) to acceptor (A). ψ_D and ψ_A are the wobbling angles of D and A, respectively. (B,C) Energy exchange process.

of available resonant energy acceptors. Therefore, the observed initial anisotropy decay with a time constant of 12 ps in sample A is mainly from the molecular wobbling motions inside of the crystal plus a small contribution from vibrational energy transfers. The observed anisotropy decay with a time constant of 1.8 ps in sample B is mainly caused by resonant energy transfers among SCN^- anions plus a small contribution from molecular wobbling.

In contrast with the resonant vibrational energy transfer from one donor to randomly orientated acceptors in liquids, which causes anisotropy to decay to zero,[4,6] the anisotropy does not decay to zero in the KSCN crystalline samples because the molecular orientations inside of the crystal are roughly confined to planes because the rotational motion (wobbling) of SCN^- is hindered, and therefore, the orientations are not random. As shown in the crystalline structure in Figure 3,[7] two adjacent anions in the KSCN crystal are either perpendicular or parallel to each other. The two shortest distances between the CN bond central points, 4.017 and 4.026 Å,[7] are both between perpendicular anion pairs (Figure 3B). In both cases, the connection lines between the central points of the CN bonds are not perpendicular to the transition dipole moment direction of either CN stretch, which is along the CN bond direction. This structure allows vibrational energy to transfer from one anion to another perpendicular anion through the second term of the dipole−dipole interaction $(\boldsymbol{\mu}\cdot\boldsymbol{\mu}/r^3 - 3(\boldsymbol{\mu}\cdot\mathbf{r})(\boldsymbol{\mu}\cdot\mathbf{r})/r^5)$.

3.2. Transfer Energy Time from One SCN^- to One Adjacent Perpendicular SCN^- 4.017 Å Away: 27 ± 3 ps.

To extract the resonant energy transfer rate constant between two CN stretches from the anisotropy measurements, we developed a kinetic model that accounts for both molecular wobbling and resonant energy transfer. As illustrated in Figure 4A, in the crystal at room temperature, the wobbling motions and vibrational energy transfers of SCN^- anions occur simultaneously with different time constants. Experimentally, by adjusting the laser intensity and spot size, only 0.1−0.5% of the anions are excited by the laser within the laser focus spot. In other words, for one energy donor, on average, there are about 200−1000 acceptors available to which energy transfer is not completely negligible. Therefore, in the kinetic model, the model sample is a small KSCN crystal with a finite number of anions. Crystals with three different sizes are used in the analyses, (1) with 108 anions (∼three layers), (2) with 500 anions (∼five layers), and (3) with 1372 anions (∼seven layers). In each small crystal, only the central SCN^- anion is the original energy donor excited by the laser, which is called the zeroth molecule (Figure 4B). Other anions are initial energy acceptors, which are called the first, second, ..., ith, and jth molecules. The vibrational energy can exchange among all anions, as illustrated in Figure 4C. Besides transferring energy, the anions can also wobble with a time constant τ_c. Both dynamic processes cause the anisotropy of the CN stretch excitation to decay. Because the wobbling motion is a hindered rotation and the orientations of the crystallites in the powder sample are random, there will be a residual anisotropy A_∞ at the infinitely long delay time.

On the basis of the physical picture described above, the CN stretch excitation probabilities are related to the experimentally measured anisotropy $r(t)$ by

$$r(t) = p_0(t)\cdot r_0(t) + p_{\parallel}(t)\cdot r_{\parallel}(t) + p_{\perp}(t)\cdot r_{\perp}(t) \tag{1}$$

where $p_0(t)$, $p_{\parallel}(t)$, and $p_{\perp}(t)$ are the vibrational excitation probabilities of the zeroth molecule, all other anions parallel to the zeroth anion, and all anions perpendicular to the zeroth anion, respectively, which are determined by the energy transfer rate constants k_{ij} between any two anions i and j. $r_0(t)$, $r_{\parallel}(t)$, and $r_{\perp}(t)$ are the anisotropy values of the zeroth SCN^-, all other SCN^- parallel to the zeroth SCN^-, and all SCN^- perpendicular to the zeroth SCN^-, respectively (detailed derivations are provided in the SI).[12,13]

$$\frac{r_0(t)}{r(0)} = \left[(1 - A_\infty)\exp\left(\frac{-t}{\tau_c}\right) + A_\infty\right] \tag{2}$$

$$\frac{r_{\parallel}(t)}{r(0)} = A_\infty\left[(1 - A_\infty)\exp\left(\frac{-t}{\tau_c}\right) + A_\infty\right] \tag{3}$$

$$\frac{r_{\perp}(t)}{r(0)} = -\left(\frac{1}{2}\right)A_\infty\left[(1 - A_\infty)\exp\left(\frac{-t}{\tau_c}\right) + A_\infty\right] \tag{4}$$

in which τ_c is the reorientational time constant and $A\infty$ is the residue reorientation anisotropy at the infinitely long delay time.

In using eq 1 to analyze the resonant vibrational energy transfer rates in the KSCN mixed crystals, only three parameters are unknown, the residue anisotropy A_∞, the reorientational time constant τ_c, and the energy transfer rate constant $(1/k_{01'})$ between the two perpendicular anions with the shortest CN distance of 4.017 Å (Figure 3B). The rate constants between any other two anions can be determined based on $1/k_{01'}$ and eqs 9−11 described in a later paragraph. Experimentally, by varying the ratio of KSCN/$KS^{13}C^{15}N$, the values of $k_{01'}$ (and therefore the total energy transfer rate constant k) and τ_c can be respectively constrained into a very small range, for example, as discussed above, the anisotropy decay time constant in the $KS^{13}C^{15}N$/KSCN = 2/98 sample must be very close to τ_c (10 ps) and that in the pure KSCN crystal must be close to $1/k$ (1.8 ps). Calculations with parameters $A_\infty = 0.70 \pm 0.06$, $1/k_{01'} = 27 \pm 3$ ps, and $\tau_c = 10.0 \pm 1$ ps simultaneously fit the experimental results of five samples (donor/acceptor = 2/98, 14/86, 35/65, 65/35, and 100/0) very well, as displayed in Figure 5. (We also calculated the time-dependent anisotropies by considering the convolution of the signal with the instrument response function and found no difference between the deconvoluted and undeconvoluted results. The results are provided in the SI.) We also found that analyses on crystals with different numbers of anions (108, 500, and 1372) give essentially the same rate constants. The difference is within 2%. This is because in the dipole/dipole interaction or higher-order interactions involved in energy transfers, the anisotropy decay is mainly the result of the energy transfers among the closest anions. All of the energy transfer time constants $1/k_{ij}$ determined with a model crystal with 500 SCN^- anions are listed in Table S2 in the SI.

3.3. Resonant Vibrational Energy Transfer Rate Determined by the Coupling Strength and Dephasing Time. The energy transfer rate constant can be theoretically correlated to the D/A distance. For the energy transfer system, the system state can be expressed as

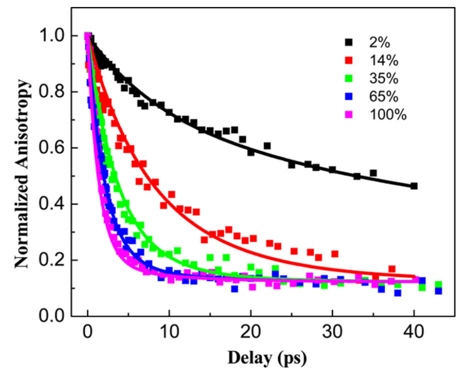

Figure 5. Time-dependent anisotropies of KSCN/$KS^{13}C^{15}N$ mixed crystals with different molar percentages of resonant energy donor species at room temperature. Dots are experimental results, and curves are calculations. Each percentage value in the figure represents the percentage of the resonant energy acceptor in each sample.

$$|\psi\rangle = c_1(t)e^{-i\omega_D t}|D = 1, A = 0\rangle + c_2(t)e^{-i\omega_A t}|D = 0, A = 1\rangle \tag{5}$$

where ω_D and ω_A are the 0−1 transition frequency of the donor and the acceptor, respectively. $|D = 1, A = 0\rangle$ is the donor state where the donor (D) is at the first excited state and the acceptor (A) is at the ground state, and $|D = 0, A = 1\rangle$ is the acceptor state where the donor (D) is at the ground state and the acceptor (A) is at the first excited state. $c_1(t)$ and $c_2(t)$ are the coefficients of these two states, with $|c_1(t)|^2 + |c_2(t)|^2 \equiv 1$. Substituting eq 5 into the time-dependent Schrödinger equation, we can obtain using the rotating wave approximation

$$c_1(t) = e^{(1/2)i\Delta\omega t}\left[\cos\left[\frac{t}{2}\sqrt{(\Delta\omega)^2 + 4\beta^2}\right] - i\frac{\Delta\omega\sin\left[\frac{t}{2}\sqrt{(\Delta\omega)^2 + 4\beta^2}\right]}{\sqrt{(\Delta\omega)^2 + 4\beta^2}}\right] \tag{6}$$

$$c_2(t) = \frac{2\beta e^{-(1/2)i\Delta\omega t}\sin\left(\frac{t}{2}\sqrt{(\Delta\omega)^2 + 4\beta^2}\right)}{\sqrt{(\Delta\omega)^2 + 4\beta^2}} \tag{7}$$

where $\Delta\omega = \omega_A - \omega_D$ and $\beta = ((\langle D = 1,A = 0|H|D = 0,A = 1\rangle/\hbar) = (\langle D = 0,A = 1|H|D = 1,A = 0\rangle/\hbar))$, where H is the system Hamiltonian. For an ensemble of D/A pairs with each pair evolving with eqs 6 and 7, the coherence is proposed to be terminated by an abrupt dephasing event at time t_c so that the D/A pair will stay in the acceptor state with probability $|c_2(t_c)|^2$. For the ensemble, the average probability on the acceptor state is $P = \int_0^\infty |c_2(t_c)|^2 p(t_c)\,dt_c$, where $p(t_c) = \tau^{-1}e^{-t_c/\tau}$ is the probability of dephasing at time t_c with $\int_0^\infty p(t_c)\,dt_c = 1$.[14] τ is the dephasing time during which the dephasing probability is equal for any time interval, and it can be determined from the energy-mismatch $(\Delta\omega)$-dependent energy transfer experiments (details are provided in the SI). The population growth rate constant of the acceptor, is therefore

$$k_p = \frac{P}{\tau} = 2\beta^2\frac{\frac{1}{\tau}}{(\Delta\omega)^2 + 4\beta^2 + \tau^{-2}} \tag{8}$$

dx.doi.org/10.1021/jp500586h | J. Phys. Chem. A 2014, 118, 2463−2469

Because the population growth rate constant is the sum of the energy transfer rate constant from the donor to the acceptor and acceptor to donor (the derivation is provided in the SI) and the rate of acceptor to donor is determined by detailed balance, the observable transfer rate constant from the donor to the acceptor is

$$k_{DA} = \frac{k_p}{1 + e^{\Delta\omega/kT}} = \frac{2}{1 + e^{\Delta\omega/kT}}\beta^2 \frac{\frac{1}{\tau}}{(\Delta\omega)^2 + 4\beta^2 + \tau^{-2}} \tag{9}$$

Equation 9 is for the weak coupling limit. In other words, it is not suitable to describe coherent energy transfers. If the coupling is weak, $(2\beta)^2 \ll \tau^{-2}$ (τ^{-2} is in energy units), and k_{DA} is proportional to β^2, which is proportional to r_{DA}^{-6} under the transition−dipole/transition−dipole interaction mechanism[2]

$$\beta^2 = \frac{1}{n^4}\frac{\mu_D^2\mu_A^2}{(4\pi\varepsilon_0)^2}\frac{\kappa^2}{r_{DA}^6} \tag{10}$$

where n is the refractive index. The local field correction factor for the refractive index[2] is not used in the analysis because all D/A pairs in the studied systems are separated by other ions (even the closest pair has K^+ cations between them). ε_0 is the vacuum permittivity. μ_D and μ_A are the transition dipole moments of the donor and acceptor respectively. r_{DA} is the distance between the donor and acceptor, which is defined as the distance between the CN center points of two SCN^- anions in the crystals. κ is the orientation factor defined in eq 11

$$\langle\kappa^2\rangle = \kappa_0^2\langle d_D\rangle\langle d_A\rangle + \frac{1}{3}(1 - \langle d_D\rangle) + \frac{1}{3}(1 - \langle d_A\rangle) + \cos^2\Theta_D\langle d_D\rangle(1 - \langle d_A\rangle) + \cos^2\Theta_A\langle d_A\rangle(1 - \langle d_D\rangle) \tag{11}$$

where $\kappa_0^2 = (\sin\Theta_D \sin\Theta_A \cos\Phi - 2\cos\Theta_D\cos\Theta_A)^2$, Θ_D, Θ_A, and Φ are the angles defined in Figure S2 (SI), and $\langle d_D\rangle = \langle d_A\rangle = (A_\infty)^{1/2}$. Equation 11 is averaged over all wobbling angles.[15] (The derivation is provided in the SI.)

Equations9−11 thus connect the resonant energy transfer rate constant k_{DA} with the D/A distance r_{DA}. All parameters in the equations are experimentally accessible.

3.4. Energy Donor/Acceptor Distance Determined to Be 3.9 ± 0.3 Å from the Transfer Time Constant. From both 1D IR and 2D IR, the transition dipole moment of the CN stretch of SCN^- in KSCN crystals was determined to be $\mu_D = \mu_A = 0.31 \pm 0.03D$. From eq 11 and XRD data and the determined $A_\infty = 0.70 \pm 0.06$, the orientation factor between the two closest SCN^- anions is determined to be $(\langle\kappa^2\rangle)^{1/2} = 0.378$. The refractive index is $n = 1.5 \pm 0.05$.[16] The dephasing time is $\tau = 0.66$ ps (8 cm^{-1}, $\tau = (1/2\pi)(100/8 \times 3)$ ps). On the basis of these experimental parameters and the energy transfer time constant $1/k_{DA} = 27 \pm 3$ ps, the calculation from eqs 9−11 gives the energy donor/acceptor distance (taken as the distance between the CN central points of the donor and acceptor because the CN stretch is mainly localized within the CN bond according to DFT calculations) $r_{DA} = 3.9 \pm 0.3$ Å. This value is very close to the XRD-determined distance of 4.017 Å.

3.5. Minor Corrections from High-Order Interactions. In calculating electronic energy transfers, if the D/A distance is comparable to the sizes of chromopores, the assumption of the point dipole in the dipole/dipole interaction can cause a significant uncertainty.[17] Corrections from higher-order interactions are needed to obtain more precise results. An efficient way to solve this problem is the monopole/monopole interaction, which counts for the charge interactions among individual atoms.[17] In the KSCN crystals studied in this work, the two closest D/A distances are about 4 Å, which is larger but not significantly larger than the CN bond length (1.1−1.2 Å). It is conceivable that higher-order interactions could matter. To address this issue, we calculated the coupling constant from the monopole/monopole interaction and found that it is only 1.3% different from that calculated from the dipole/dipole interaction, which is the first-order approximation of the monopole/monopole interaction. The calculations show that the higher-order interactions play minor roles in the systems studied. Detailed calculations are provided in the SI.

3.6. Anion Distances in Ion Clusters in KSCN Aqueous Solutions: r_{DA} = 4.4 ± 0.4 Å. Using eqs 9−11 to determine angstrom distances from vibrational energy transfer rate constants is not limited only to solid samples. The approach is also applicable for liquids. We have determined that in the 1 and 1.8 M KSCN aqueous solutions, more than 25% of the ions form clusters, and on average, the clusters contain three (1 M) and four (1.8 M) SCN^- anions.[4] The resonant one-donor-to-one-acceptor energy transfer time constants were determined to be 15 (1 M) and 18 ps (1.8 M), respectively (Figures S6 and S7 in the SI), based on the method introduced previously.[4] The transfer time in the 1.8 M solution seems slightly slower than that in the 1 M solution, but the difference is within the experimental uncertainty. On the basis of these energy transfer time constants and eqs 9−11, the distances between two SCN^- anions in the clusters in the two solutions are determined to be $r_{DA} = 4.4 \pm 0.4$ Å. Calculation details and experimental data are provided in the SI. The determined clustered anion distances are significantly shorter than the average anion distance (∼1 nm) in the aqueous solutions if ion clustering did not occur but very close to the four closest anion distances (4.0 Å) in the KSCN crystal. The result suggests that the ions inside of the clusters have direct contact with each other.

4. CONCLUDING REMARKS

The results presented in the work demonstrate the potential of using vibrational energy transfers as a ruler to determine both static and transient intermolecular distances at the angstrom scale in both liquid and solid samples. The results also show that ions can form direct-contact ion clusters in relatively dilute strong electrolyte aqueous solutions. We expect that the studies of many fundamental problems in various fields will benefit from applying the vibrational energy transfer method, for example, the prenucleation of ions or molecules during the growth of crystals and nanomaterials, the formations of minerals in nature and bioinorganic composites (shells and bones) in living creatures, and the ion/biomolecular interactions. To achieve the ultimate goal of an “angstrom molecular ruler”, many more studies on more delocalized systems with shorter D/A distances and various D/A energy mismatches are needed. Advances in laser and detection technology for the fingerprint frequency region below 1000 cm^{-1} are also highly desirable for more sophisticated molecular systems.

■ ASSOCIATED CONTENT

Ⓢ Supporting Information

Supporting figures and data about FTIR, 2D-IR measurements, detailed derivation of equations, and data analyses. This material is available free of charge via the Internet at http://pubs.acs.org.

■ AUTHOR INFORMATION

Corresponding Author

*E-mail: junrong@rice.edu.

Author Contributions

[†]H.C. and X.W. contributed equally to the work.

Notes

The authors declare no competing financial interest.

■ ACKNOWLEDGMENTS

This material is based upon work supported by the Welch foundation under Award No. C-1752 and AFOSR Award No. FA9550-11-1-0070. J.Z. also thanks the David and Lucile Packard Foundation for a Packard fellowship. Insightful discussions with Profs. Robert, F. Curl, Anatoly B. Kolomeisky, David Jonas, Greg Angel, Qiang Shi, and Donghui Zhang are appreciated.

■ REFERENCES

(1) Förster, T. Zwischenmolekulare Energiewanderung Und Fluoreszenz. *Ann. Phys.* **1948**, *437*, 55−75.
(2) Scholes, G. D. Long-Range Resonance Energy Transfer in Molecular Systems. *Annu. Rev. Phys. Chem.* **2003**, *54*, 57−87.
(3) Bian, H. T.; Li, J. B.; Wen, X. W.; Zheng, J. R. Mode-Specific Intermolecular Vibrational Energy Transfer. I. Phenyl Selenocyanate and Deuterated Chloroform Mixture. *J. Chem. Phys.* **2010**, *132*, 184505.
(4) Bian, H. T.; Wen, X. W.; Li, J. B.; Chen, H. L.; Han, S. Z.; Sun, X. Q.; Song, J. A.; Zhuang, W.; Zheng, J. R. Ion Clustering in Aqueous Solutions Probed with Vibrational Energy Transfer. *Proc. Natl. Acad. Sci. U.S.A.* **2011**, *108*, 4737−4742.
(5) Bian, H.; Chen, H.; Li, J.; Wen, X.; Zheng, J. Nonresonant and Resonant Mode-Specific Intermolecular Vibrational Energy Transfers in Electrolyte Aqueous Solutions. *J. Phys. Chem. A* **2011**, *115*, 11657−11664.
(6) Woutersen, S.; Bakker, H. J. Resonant Intermolecular Transfer of Vibrational Energy in Liquid Water. *Nature* **1999**, *402*, 507−509.
(7) Akers, C.; Peterson, S. W.; Willett, R. D. A Refinement of Crystal Structure of KSCN. *Acta Crystallogr., Sect. B* **1968**, *24*, 1125−1126.
(8) Cookson, D.; Finlayson, T.; Elcombe, M. Phonon Dispersion Relations for Potassium Thiocyanate. *Solid State Commun.* **1987**, *64*, 357−359.
(9) Cookson, D.; Elcombe, M.; Finlayson, T. Phonon Dispersion Relations for Potassium Thiocyanate at and above Room Temperature. *J. Phys.: Condens. Matter* **1992**, *4*, 7851−7864.
(10) Nagy, S. *Radiochemistry and Nuclear Chemistry*; Eolss Publishers Company Limited: Oxford, U.K., 2009.
(11) Lakowicz, J. *Principles of Fluorescence Spectroscopy*, 3rd ed.; Springer: New York, 2006.
(12) Kinosita, K.; Kawato, S.; Ikegami, A. A Theory of Fluorescence Polarization Decay in Membranes. *Biophys. J.* **1977**, *20*, 289−305.
(13) Lipari, G.; Szabo, A. Effect of Librational Motion on Fluorescence Depolarization and Nuclear Magnetic Resonance Relaxation in Macromolecules and Membranes. *Biophys. J.* **1980**, *30*, 489−506.
(14) Curl, R. F.; Kasper, J. V. V; Pitzer, K. S. Nuclear Spin State Equilibration through Nonmagnetic Collisions. *J. Chem. Phys.* **1967**, *46*, 3220−3228.
(15) Dale, R. E.; Eisinger, J.; Blumberg, W. The Orientational Freedom of Molecular Probes. The Orientation Factor in Intramolecular Energy Transfer. *Biophys. J.* **1979**, *26*, 161−193.
(16) Savoie, R.; Tremblay, J. Raman Spectra of Crystals Immersed in Liquids. *J. Opt. Soc. Am.* **1967**, *57*, 329−332.
(17) Chang, J. C. Monopole Effects on Electronic Excitation Interactions between Large Molecules. I. Application to Energy Transfer in Chlorophylls. *J. Chem. Phys.* **1977**, *67*, 3901−3909.

Supporting Information

Molecular distance determined with resonant vibrational energy transfer

Hailong Chen[†], Xiewen Wen[†], Jiebo Li, Junrong Zheng*

Department of Chemistry, Rice University, Houston, TX

† These authors contributed equally to the work

*To whom correspondence should be addressed: junrong@rice.edu

Optical image of the sample

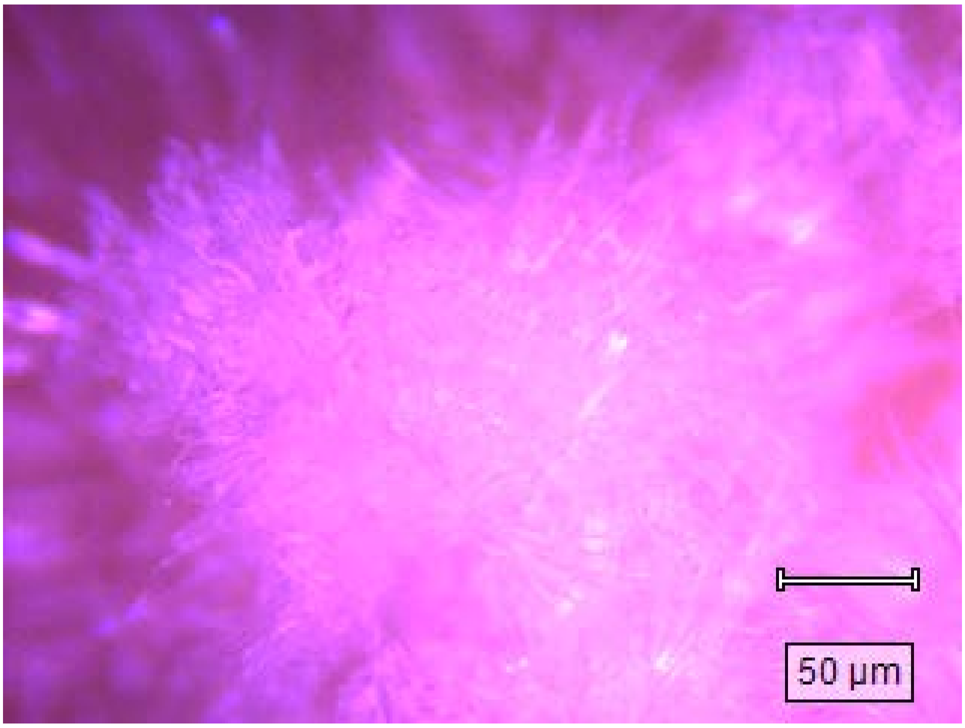

Figure S1. *Optical image of the KSCN polycrystalline sample mixed with 50% PMMA.*

Calculation details of fig.2

For the KSCN:KS^{13}C^{15}N = 1:1 non-resonant energy transfer experiments shown in fig.2 in the main text, we have a kinetic model [1]

$$\xleftarrow{k_{S^{13}C^{15}N^-}}[S^{13}C^{15}N^-]\underset{k_{SCN^-\to S^{13}C^{15}N^-}}{\overset{k_{S^{13}C^{15}N^-\to SCN^-}}{\rightleftarrows}}[SCN^-]\xrightarrow{k_{SCN^-}}$$

where [S^{13}C^{15}N$^-$] denotes the population of excited S^{13}C^{15}N$^-$ anion, and [SCN$^-$] denotes the population of excited SCN$^-$ anion. $k_{S^{13}C^{15}N^-\to SCN^-}$ represents the energy transfer rate constant from S^{13}C^{15}N$^-$ to SCN$^-$ and $k_{SCN^-\to S^{13}C^{15}N^-}$ represents the transfer rate constant from SCN$^-$ to S^{13}C^{15}N$^-$. $k_{S^{13}C^{15}N^-}$ and k_{SCN^-} are the vibrational lifetimes of S^{13}C^{15}N$^-$ and SCN$^-$, respectively.

According to the scheme, we have kinetic equations:

$$\begin{cases} \dfrac{d[SCN^-]}{dt} = -k_{SCN^-}[SCN^-] + k_{S^{13}C^{15}N^-\to SCN^-}[S^{13}C^{15}N^-] - k_{SCN^-\to S^{13}C^{15}N^-}[SCN^-] \\ \dfrac{d[S^{13}C^{15}N^-]}{dt} = -k_{S^{13}C^{15}N^-\to SCN^-}[S^{13}C^{15}N^-] + k_{SCN^-\to S^{13}C^{15}N^-}[SCN^-] - k_{S^{13}C^{15}N^-\to SCN^-}[S^{13}C^{15}N^-] \end{cases} \quad . \qquad \text{eq.S1}$$

In the equations, the time dependent populations were obtained from the vibrational energy exchange measurements. The lifetimes were determined by pump/probe experiments. The rate ratio $\frac{k_{S^{13}C^{15}N^-\to SCN^-}}{k_{SCN^-\to S^{13}C^{15}N^-}} = e^{-\frac{75}{200}} = 0.69$ is determined by the detailed balanced principle. In analyzing the energy exchange rates with eqs.1, we had only one unknown parameter, $k_{SCN^-\to S^{13}C^{15}N^-}$. Calculation results with $k_{SCN^-\to S^{13}C^{15}N^-} = 1/(99 \pm 5)\text{ ps}$, $k_{S^{13}C^{15}N^-\to SCN^-} = 1/(140 \pm 7)\text{ ps}$, $k_{SCN^-} = 525 \pm 45\text{ ps}$, $k_{S^{13}C^{15}N^-} = 585 \pm 50\text{ ps}$ fit the four experimental curves very well, as shown in fig.2 E&F. The analysis gives the energy transfer time constant from S^{13}C^{15}N$^-$ to SCN$^-$, $\frac{1}{k_{S^{13}C^{15}N^-\to SCN^-}} = 140 \pm 7\text{ps}$.

The derivation of orientation factor κ

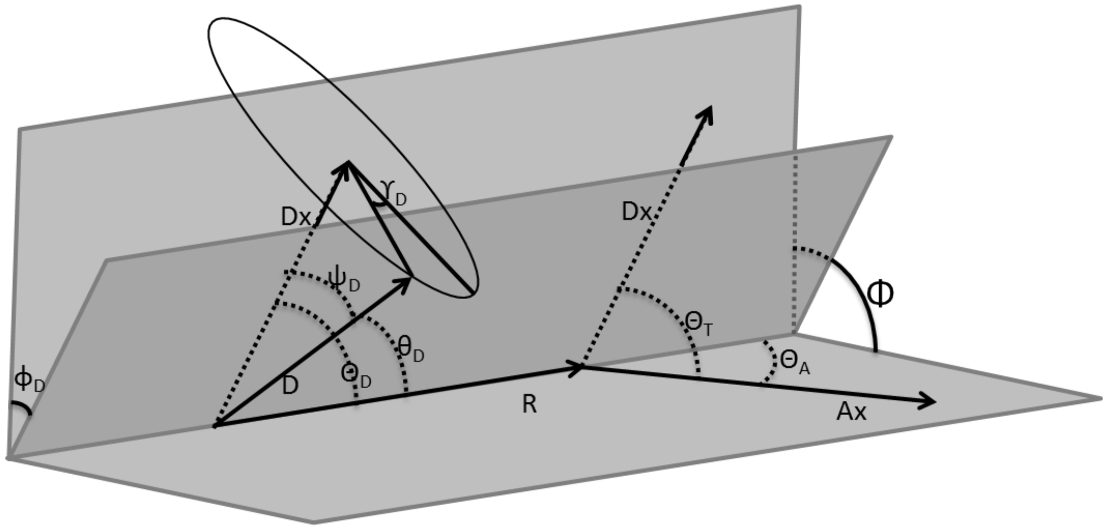

Figure S2. *Illustration of Donor and acceptor dipole moment orientations. D_x and A_x are the symmetry axes of their distributions, D is the wobbling donor vector, ψ_D, θ_D, γ_D represent the azimuth angles. For neatness, wobbling acceptor vector A is not shown in the figure, and ψ_A, θ_A, γ_A represent the corresponding angles.*

For random donor (D) and acceptor (A) orientations, the orientation factor is

$$\kappa_i^2 = (\sin\theta_D \sin\theta_A \cos\phi - 2\cos\theta_D \cos\theta_A)^2 , \qquad \text{eq.S2}$$

where θ_D and θ_A are the angles between each transition dipole moment and the vector connecting them, and the azimuth angle is

$$\phi = \Phi + \phi_A - \phi_D . \qquad \text{eq.S3}$$

The orientation of D is related to A by the following identities

$$\sin\phi_D \cos\phi_D = \sin\Theta_D \cos\psi_D - \cos\Theta_D \sin\psi_D \cos\gamma_D \qquad \text{eq.S4}$$

$$\cos\theta_D = \cos\Theta_D \cos\psi_D + \sin\Theta_D \sin\psi_D \cos\gamma_D \qquad \text{eq.S5}$$

$$\sin\phi_A \cos\phi_A = \sin\Theta_A \cos\psi_A - \cos\Theta_A \sin\psi_A \cos\gamma_A \qquad \text{eq.S6}$$

$$\cos\theta_A = \cos\Theta_A \cos\psi_A + \sin\Theta_A \sin\psi_A \cos\gamma_A . \qquad \text{eq.S7}$$

Substituting eq.S4~7 into eq.S2 and averaging over the dynamic azimuthal angles γ_D

and γ_A, we obtain $\langle \cos\gamma \rangle = \langle \sin\gamma \rangle = \langle \cos\gamma \sin\gamma \rangle = 0$ and

$\langle \cos^2\gamma \rangle = \langle \sin^2\gamma \rangle = 1/2$.

eq.S8

Over the appropriate ranges of γ_D and γ_A, one sees that the (dynamic) average value of the orientation factor is

$$\begin{aligned}\left\langle \kappa^2 \right\rangle &= \kappa_0^2 \left\langle d_D \right\rangle \left\langle d_A \right\rangle + \frac{1}{3}(1 - \left\langle d_D \right\rangle) + \frac{1}{3}(1 - \left\langle d_A \right\rangle) \\ &+ \cos^2\Theta_D \left\langle d_D \right\rangle (1 - \left\langle d_A \right\rangle) + \cos^2\Theta_A \left\langle d_A \right\rangle (1 - \left\langle d_D \right\rangle)\end{aligned} \quad , \qquad \text{eq.S9}$$

where $\left\langle d_D \right\rangle = \left\langle P_2(\cos\psi_D) \right\rangle$, $\left\langle d_A \right\rangle = \left\langle P_2(\cos\psi_A) \right\rangle$, with $P_2(x) = (3x^2 - 1)/2$ is the second Legendre polynomial, and

$\kappa_0^2 = (\sin\Theta_D \sin\Theta_A \cos\Phi - 2\cos\Theta_D \cos\Theta_A)^2$.

eq.S10

In next section, we'll derive $\left\langle d_D \right\rangle = \left\langle d_A \right\rangle = \sqrt{A_\infty}$, where A_∞ is the residue reorientation anisotropy value at the infinitely long waiting time.

Anisotropy of parallel and perpendicular anions

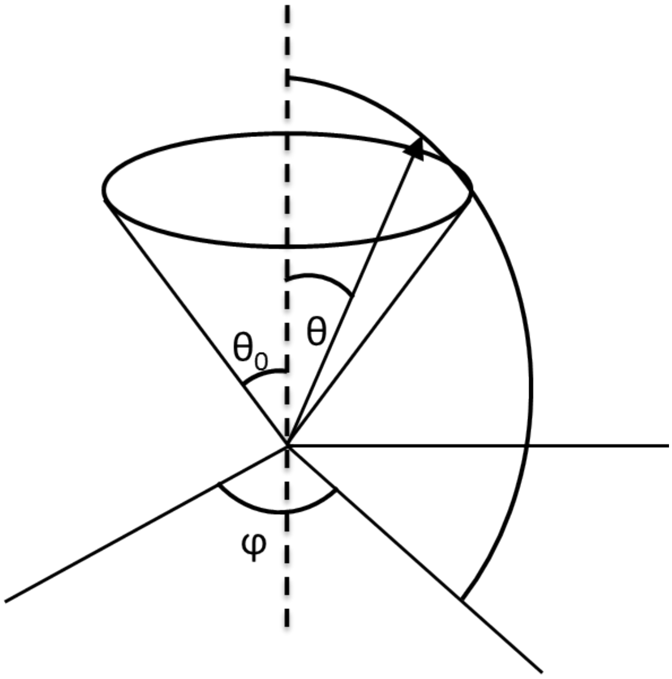

Figure S3. *Illustration of wobbling model, the dipole symmetry axis wobbles within a cone of semiangle* θ_0

The definition of anisotropy is

$$r(t) = \frac{I_{\parallel}(t) - I_{\perp}(t)}{I_{\parallel}(t) + 2I_{\perp}(t)}, \qquad \text{eq.S11}$$

in which $I_{\parallel}(t)$ and $I_{\perp}(t)$ are the pump probe signals with the detection polarizations are respectively parallel and perpendicular to the excitation .

Similar to the results that had been derived for librational motion on fluorescence depolarization [2], $r(t)$ can be expressed in terms of a correlation function as

$$r(t) = r(0) \cdot \left\langle P_2[\boldsymbol{\mu}(0) \cdot \boldsymbol{\mu}(t)] \right\rangle, \qquad \text{eq.S12}$$

where $\boldsymbol{\mu}(0)$ and $\boldsymbol{\mu}(t)$ are the unit transition dipole vector at time 0 and t, respectively. $r(0)$ is the initial anisotropy of the total signal, the angular brackets denote an equilibrium average, and $P_2(x) = (3x^2 - 1)/2$ is the second Legendre polynomial.

To determine $r(\infty)$ we use the addition theorem for the spherical harmonics [2], and rewrite eq.S12 as

$$r(t) = r(0) \sum_{m=-2}^{2} \left\langle C_{2m}^{*}[\theta(0), \phi(0)] C_{2m}[\theta(t), \phi(t)] \right\rangle, \qquad \text{eq.S13}$$

where $C_{lm}(\theta,\phi)$ are the modified spherical harmonics, and the spatial angles θ and ϕ specify the orientation of dipole moment. When $t \to \infty$, $\lim_{t\to\infty}\langle A(0)B(t)\rangle = \langle A\rangle\langle B\rangle$, therefore, the residue reorientation anisotropy at the infinitely long waiting time

$$A_\infty \equiv \frac{r(\infty)}{r(0)} = |\langle C_{20}\rangle|^2 = \langle P_2(\cos\theta)\rangle^2, \qquad \text{eq.S14}$$

where θ is the angle between dipole and its symmetry axis, and $\langle P_2(\cos\theta)\rangle$ can be determined by the wobbling angle θ_0 by [2]

$$\langle P_2(\cos\theta)\rangle = \frac{1}{2}\cos\theta_0(1+\cos\theta_0) \qquad . \qquad \text{eq.S15}$$

Therefore, we can obtain the wobbling angle from the measured value of residue anisotropy by the expression

$$A_\infty = \left[\frac{1}{2}\cos\theta_0(1+\cos\theta_0)\right]^2 \qquad . \qquad \text{eq.S16}$$

For the 0th SCN^- anion (see Figs. 4B and 4C), time dependent anisotropy caused by its rotation is single exponential with a residue [2,3]:

$$\frac{r_0(t)}{r(0)} = \langle P_2[\cos\theta(t)]\rangle^2 = (1-A_\infty)\exp(-t/\tau_c) + A_\infty \quad , \qquad \text{eq.S17}$$

where τ_c is the rotational time constant. For the other anions, which act as energy acceptors, their anisotropy values can be calculated as follow.

According to Soleillet's theorem, if a series of depolarizing events intervenes between absorption and emission and each reorientation is azimuthally isotropic with respect to the preceding one, the anisotropy can be written as [4,5]

$$r = 0.4\prod_i \langle P_2(\cos\theta_i)\rangle, \qquad \text{eq.S18}$$

where θ_i is the angle by which the transition moment is changed in the *i*th depolarization step.

It was demonstrated, the transfer depolarization process depicted in Fig.4A is entirely equivalent to the reorientation of D_i to the axial orientation D_x followed by the transfer to the acceptor in its axial orientation A_x and reorientation to A_j [5]. Since D_x and A_x are axially symmetrically distributed about D_x and A_x, respectively, and the azimuthal orientation of A_x about D_x (being a particular case of A_j about D_i) is random, Soleillet's theorem applies, and the average transfer depolarization factor is the product of the three depolarization factors, corresponding to the three depolarizing events described above. Therefore, we have,

$$\begin{aligned}\frac{r(t)}{r(0)} &= \left\langle P_2[\cos\theta_{D_iD_j}(t_i)]\right\rangle \left\langle P_2[\cos\theta_{D_jA_i}(t_i)]\right\rangle \left\langle P_2[\cos\theta_{A_iA_j}(t-t_i)]\right\rangle \\ &\approx R_{rot}(t)\left\langle P_2(\cos\psi_D)\right\rangle P_2(\cos\Theta_T)\left\langle P_2(\cos\psi_A)\right\rangle\end{aligned} \quad , \qquad \text{eq.S19}$$

where ψ_D, ψ_A and Θ_T were defined in Fig.S2, and we have demonstrated $\left\langle P_2(\cos\psi_D)\right\rangle = \left\langle P_2(\cos\psi_A)\right\rangle = \sqrt{A_\infty}$, and $R_{rot}(t) = (1-A_\infty)\exp(-t/\tau_c) + A_\infty$ (see eq.S15).

According to eq.S19, for the anions with direction parallel to 0th, $\Theta_T = 0$, and

$$\begin{aligned}\frac{r_{\parallel}(t)}{r(0)} &= R_{rot}(t)A_\infty P_2(\cos 0) \\ &= A_\infty[(1-A_\infty)\exp(-t/\tau_c) + A_\infty]\end{aligned} \quad , \qquad \text{eq.S20}$$

For anions perpendicular to 0th anion, similarly,

$$\begin{aligned}\frac{r_{\perp}(t)}{r(0)} &= R_{rot}(t)A_\infty P_2(\cos\pi) \\ &= -\frac{1}{2}A_\infty[(1-A_\infty)\exp(-t/\tau_c) + A_\infty]\end{aligned} \quad , \qquad \text{eq.S21}$$

Deconvolution results of waiting time dependent anisotropies in fig. 5

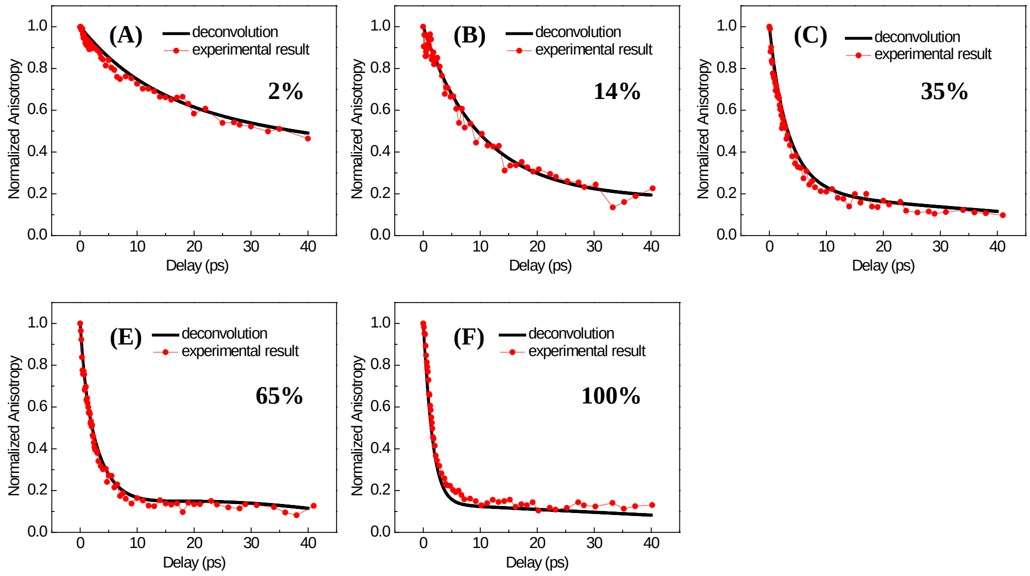

Figure S4. *Deconvolution results of waiting time dependent anisotropies of KSCN/KS^{13}C^{15}N mixed crystals with different molar percentages of resonant energy donor species at room temperature. The experimental results are from fig.5. The deconvolution results were obtained by fitting the parallel and perpendicular polarized pump/probe signal respectively in consideration of the convolution with the instrument response function,*[6] *and then followed by the calculation of anisotropy.*

FTIR measurement and lineshape fitting

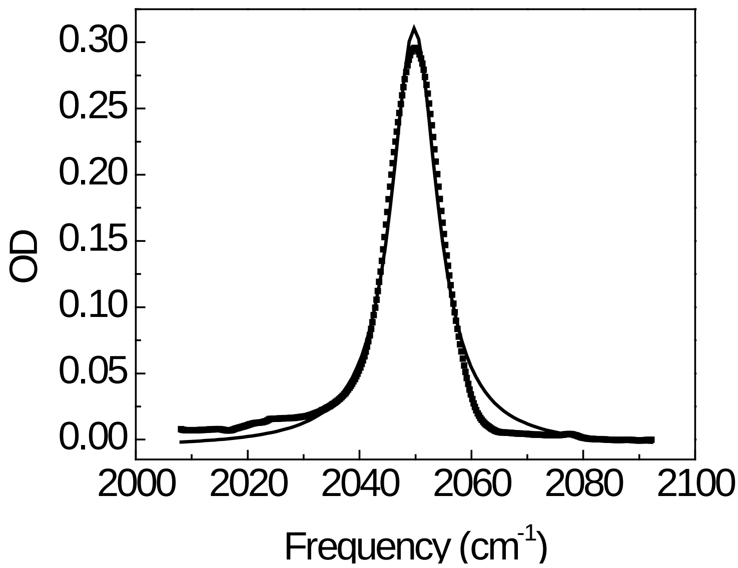

Figure S5. *FTIR spectrum of the KSCN crystal. The square dots are experimental data, and the solid line is the fitting result with a Lorentzian.*

Figure S5 is the FTIR spectrum of KSCN crystal in the CN stretch vibrational frequency range. It can be fit with a Lorentzian very well. The Lorentzian lineshape has a function form of

$$y = y_0 + \frac{2A\pi w}{4(w - w_c)^2 + w^2}, \qquad \text{eq.S22}$$

where w is the Lorentzian linewidth, all fitting parameters are $y_0 = -0.0063,\ x_c = 2049.79,\ w = 9.96,\ A = 4.96$.

Correction from high order interactions - monopole approximation, description and calculation

According to the transition monopole approximation, the interaction matrix can be obtained by considering the detailed interaction between the effective electron charges ("monopoles") in the transition moment located at the equilibrium positions of the nuclei of the atoms. By making use of the zero-differential overlap approximation, and the point charge approximation for two center atomic Coulomb integrals, the interaction matrix element can be written as [7]

$$U^{AB} \sim U_M = \sum_{i,j=1}^{N_A} (CM)_{i,e}^{A} (CM)_{j,e}^{B} 1/\varepsilon \left| \mathbf{R}_i^A - \mathbf{R}_j^B \right| \quad , \qquad \text{eq.S23}$$

where $\mathbf{R}_i^A$ and $\mathbf{R}_j^B$ are the nuclear equilibrium positions of the *i*th atom of molecule *A* and the *j*th atom of molecule *B*, respectively. N_A is the total number of atoms which contribute electrons, ε is dielectric constant, and $(CM)_{i,e}^{A}$ is the transition monopole in molecule, which was defined as the transition charge located at the equilibrium position R_i of atom *i* in the molecule when it is undergoing a transition between the ground and excited states.

Eq. S23 can be expanded in Taylor series about **R**, with the dipole interaction as the lowest order, i.e.

$$U_D = \sum_{i,j=1}^{N_A} (CM)_{i,e}^{A} (CM)_{j,e}^{B} [\mathbf{R}_{iA}^0 \cdot \mathbf{R}_{jB}^0 - 3(\mathbf{R}_{iA}^0 \cdot \mathbf{R})(\mathbf{R}_{jB}^0 \cdot \mathbf{R}) / R^2] / \varepsilon R^3 \qquad \text{eq.S24} ,$$

where $\mathbf{R}_{iA}^0$ is the nuclear equilibrium position of the *i*th atom in molecule *A* with reference to the center of molecule *A*, $\mathbf{R}_{jB}^0$ is defined similarly, and **R** is distance vector from the center of *A* to the center of *B* with *R* is the distance.

Considering the interaction between two CN stretching modes located on different molecules in KSCN crystal, there are only two atoms (C and N) involved in the vibration for each of the molecule, therefore, $N_A = 2$, *i*, *j* = C or N, and the transition monopoles have the relation: $(CM)_{C,e}^{A} = (CM)_{C,e}^{B} = -(CM)_{N,e}^{A} = -(CM)_{N,e}^{B} = C$, with C is a transition charge constant.

Eqs. S23 and S24 can be calculated by substituting all the related coordinates of C and N atoms (with the unit of Å) according to the crystal structure of KSCN, e.g. for a pair of CN with the strongest coupling, we have (without considering the wobbling):

Table S1. *Calculation parameters and results for the pair of CN with the strongest coupling*

$\mathbf{R}_C^A$	(5.16, 1.96, 1.89)	$\mathbf{R}_{CA}^0$	(-0.399, -0.410, 0)	$\mathbf{R}$	(2.22, 3.36, 0)
$\mathbf{R}_N^A$	(5.96, 2.78, 1.89)	$\mathbf{R}_{NA}^0$	(0.399, 0.410, 0)	R	4.026
$\mathbf{R}_C^B$	(8.18, 5.32, 1.89)	$\mathbf{R}_{CB}^0$	(0.399, -0.410, 0)	$\lvert U^{AB}\rvert$	0.01218 C^2
$\mathbf{R}_N^B$	(7.38, 6.14, 1.89)	$\mathbf{R}_{NB}^0$	(-0.399, 0.410, 0)	$\lvert U_D\rvert$	0.01202 C^2

Therefore, the deviation of the coupling calculated with the dipole interaction from that calculated with the transition monopole approximation is $(\lvert U^{AB}\rvert - \lvert U_D\rvert)/\lvert U_D\rvert = 1.3\%$.

Vibrational excitation probabilities of parallel and perpendicular anions

As illustrated in fig.4B&4C, in each small crystal, only the central SCN^- anion is the original energy donor excited by the laser, which is called the 0^{th} molecule. Other anions are initial energy acceptors. The vibrational energy can exchange among all anions. As a result, the resonant vibrational energy transfer kinetics can be expressed as

$$\frac{dp_0(t)}{dt} = \sum_j k_{j0} p_j(t) + \sum_{j'} k_{j'0} p'_{j'}(t) - \sum_j k_{0j} p_0(t) - \sum_{j'} k_{0j'} p_0(t) \qquad \text{eq.S25}$$

$$\frac{dp_i(t)}{dt} = \sum_{j \neq i} k_{ji} p_j(t) + \sum_{j'} k_{j'i} p'_{j'}(t) - \sum_{j \neq i} k_{ij} p_i(t) - \sum_{j'} k_{ij'} p_i(t) \qquad \text{eq.S26}$$

$$\frac{dp'_{i'}(t)}{dt} = \sum_{j' \neq i'} k_{j'i'} p'_{j'}(t) + \sum_j k_{ji'} p_j(t) - \sum_{j' \neq i'} k_{i'j'} p'_{i'}(t) - \sum_j k_{i'j} p'_{i'}(t) \qquad \text{eq.S27}$$

where p_i and k_{ij} are the probability of vibrational excitation of anion *i* and the vibrational energy transfer rate constant from anion *i* to anion *j* respectively. k_{ij} is correlated to each other through eq.9&10. In the equations, the $'$ mark represents the anions perpendicular to the 0^{th} anion. The anions parallel to the 0^{th} anion are represented by the regular symbols. Eqs.S25-S27 respectively describe the time dependent probability of vibrational excitation of the 0^{th} molecule, an anion parallel to the 0^{th} anion, and an anion perpendicular to the 0^{th} molecule. For the total excitation probability of all the anions parallel or perpendicular to the 0^{th} molecule, we have

$$\begin{aligned}\frac{dp_{\parallel}(t)}{dt} &= \sum_{i \neq 0} \frac{dp_i(t)}{dt} \\ &= \sum_{i \neq 0} \sum_j k_{ji} p_j(t) + \sum_{j'} p'_{j'}(t) \sum_{i \neq 0} k_{j'i} - \sum_{i \neq 0} \sum_j k_{ij} p_i(t) - \sum_{i \neq 0} \sum_{j'} k_{ij'} p_i(t)\end{aligned}$$

eq.S28

$$\begin{aligned}\frac{dp_{\perp}(t)}{dt} &= \sum_{i'} \frac{dp'_{i'}(t)}{dt} \\ &= \sum_{i'} \sum_{j'} k_{j'i'} p'_{j'}(t) + \sum_j p_j(t) \sum_{i'} k_{ji'} - \sum_{i'} \sum_{j'} k_{i'j'} p'_{i'}(t) - \sum_{i'} \sum_j k_{i'j} p'_{i'}(t)\end{aligned} \qquad \text{eq.S29}$$

For the same surroundings of the molecules in crystal, the total energy transfer rate constant from the 0^{th} anion to all parallel anions is $k_{\parallel} = \sum_i k_{ji} = \sum_{i'} k_{j'i'} = \sum_j k_{ij} = \sum_{j'} k_{i'j'}$, and the total energy transfer rate constant from the 0^{th} anion to all perpendicular anions is $k_{\perp} = \sum_i k_{j'i} = \sum_{i'} k_{ji'} = \sum_{j'} k_{ij'} = \sum_j k_{i'j}$. The excitation probability of all anions parallel to the 0^{th} anion is $p_{\parallel}(t) = \sum_{i \neq 0} p_i(t)$, and the

excitation probability of all anions perpendicular to the 0th anion is $p_{\perp}(t)=\sum_{i'\neq 0} p_{i'}(t)$.
For samples mixed with $KS^{13}C^{15}N$, the total resonant energy transfer rate constant of SCN^- is $k_c = ck = c(k_{\|}+k_{\perp})$, where *c* is the percentage of KSCN in a mixed crystal.

Eq. S25, S28 and S29 can be rewritten as

$$\frac{dp_0(t)}{dt}=\sum_j k_{j0}p_j(t)+\sum_{j'} k_{j'0}p'_{j'}(t)-k_{\|}p_0(t)-k_{\perp}p_0(t) \qquad \text{eq.S30}$$

$$\frac{dp_{\|}(t)}{dt}=k_{\|}p_0(t)+k_{\perp}p_{\perp}(t)-k_{\perp}p_{\|}(t)-\sum_j k_{j0}p_j(t)-\sum_{j'} k_{j'0}p_{j'}(t) \qquad \text{eq.S31}$$

$$\frac{dp_{\perp}(t)}{dt}=k_{\perp}p_0(t)+k_{\perp}p_{\|}(t)-k_{\perp}p_{\perp}(t) \qquad \text{eq.S32}$$

With the initial conditions $p_0(0)=1$, and $p_{\|}(0)=p_{\perp}(0)=0$, using a strategy in literature [8,9] for a large number of acceptors ($j, j' >> 2$), eqs.S30~32 can be numerically solved with

$$p_0(t)\approx\prod_j\frac{1+e^{-2k_{0j}t}}{2}\prod_{j'}\frac{1+e^{-2k_{0j'}t}}{2} \qquad \text{eq.S33}$$

$$p_{\|}(t)\approx\frac{1}{2}+\frac{1}{2}e^{-2k_{\perp}t}-\prod_j\frac{1+e^{-2k_{0j}t}}{2}\prod_{j'}\frac{1+e^{-2k_{0j'}t}}{2} \qquad \text{eq.S34}$$

$$p_{\perp}(t)=\frac{1}{2}-\frac{1}{2}e^{-2k_{\perp}t}, \qquad \text{eq.S35}$$

where k_{ij} and $k_{ij'}$ are correlated to each other through eqs.13&14 in the main text.

Calculations of clustered anion distances in 1M and 1.8M KSCN aqueous solutions

We have the parameters: $n = 1.5$, $\mu_D = \mu_A = 0.33D$, $\langle \kappa \rangle = \sqrt{2/3}$ (randomized, because the rotation of anion is faster than the energy transfer) and the dephasing time $\tau = 0.29\ ps$ ($\tau = \frac{1}{2\pi}\frac{100}{18\times 3}ps$) for the 1.8M solution and $\tau = 0.27\ ps$ ($\tau = \frac{1}{2\pi}\frac{100}{20\times 3}ps$) for the 1M solution from the energy mismatch dependent experiments (fig.S6~7) [1,10].

For the 1.8 M solution

$$k = \beta^2 \frac{\frac{1}{\tau}}{(2\beta)^2 + \tau^{-2}} = \frac{1}{18ps} \qquad \Rightarrow \beta = 2.3\ cm^{-1}$$

$$\beta = \frac{1}{n^2}\frac{\mu_D \mu_A}{4\pi\varepsilon_0}\frac{\kappa}{r_{DA}^3} \qquad \Rightarrow r_{DA} = 4.4\ \dot{\mathrm{A}}$$

For the 1M solution

$$k = \beta^2 \frac{\frac{1}{\tau}}{(2\beta)^2 + \tau^{-2}} = \frac{1}{15ps} \qquad \Rightarrow \beta = 2.5\ cm^{-1}$$

$$\beta = \frac{1}{n^2}\frac{\mu_D \mu_A}{4\pi\varepsilon_0}\frac{\kappa}{r_{DA}^3} \qquad \Rightarrow r_{DA} = 4.3\ \dot{\mathrm{A}}$$

If n = 1.42 is used (averaging the refractive indexes of D_2O and KSCN), $r_{DA} = 4.5\ \dot{\mathrm{A}}$ and $r_{DA} = 4.4\ \dot{\mathrm{A}}$ are for the 1.8M and 1M solutions respectively.

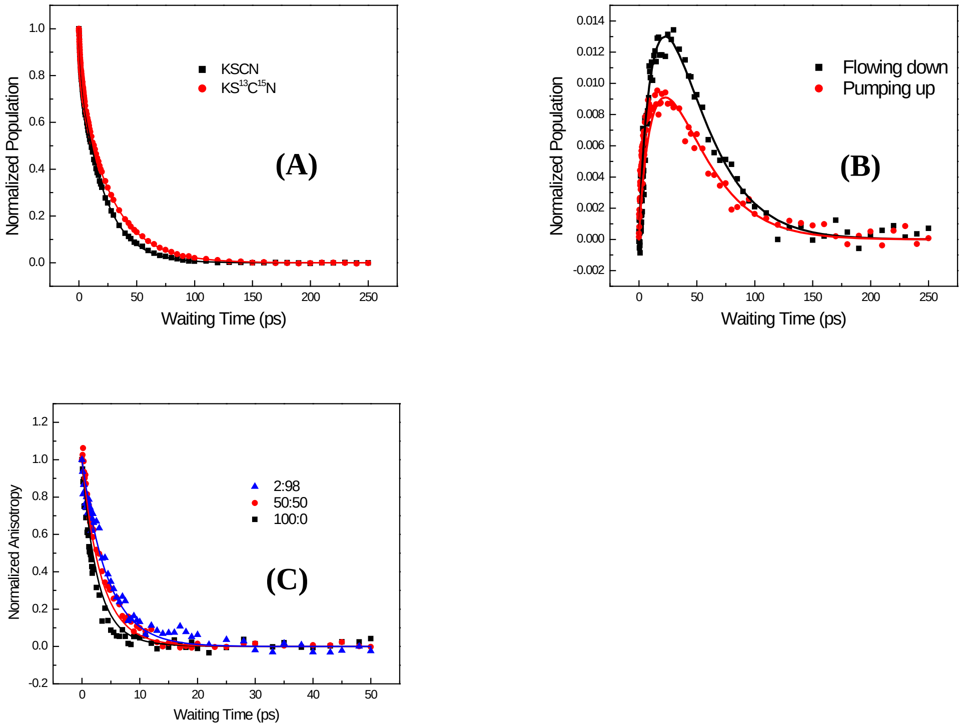

Figure S6. *Data and calculations of nonresonant [(A) and (B)] energy transfer between SCN⁻ and $S^{13}C^{15}N^-$ ($SCN^-/S^{13}C^{15}N^-$=1/1) and resonant [(C)] energy transfers among SCN⁻ anions for a 1.8M KSCN aqueous solution from our previous publication.*[1] *Dots are data, and lines are calculations. Calculations for (A) and (B) are with input parameters:*

$$k_{SCN^- fast}=1/1.4\ (ps^{-1});\ k_{SCN^- slow}=1/22\ (ps^{-1});\ k_{S^{13}C^{15}N^- fast}=1/2.7\ (ps^{-1});\ k_{S^{13}C^{15}N^- slow}=1/29\ (ps^{-1});$$

$$k_{clu\to iso}=1/10\ (ps^{-1});\ \text{K=0.55};\ k_{SCN^-\to S^{13}C^{15}N^-}=1/160\ (ps^{-1});\ \text{D=0.70}$$

with pre-factors of the subgroups and offset of the bi-exponential

$$A_{SCN^- fast}=0.16;\ A_{SCN^- slow}=0.84;\ A_{S^{13}C^{15}N^- fast}=0.22;\ A_{S^{13}C^{15}N^- slow}=0.78;\ offset=0\,.$$

(C) $\tau_{or}=4.5ps$ *is experimentally determined, which is the rotation time of the clustered ions.* $n_{tot}=4$, $\tau=18ps$. Therefore, for the same number of acceptors, the resonant transfer time is 18/2=9ps, and that for $\Delta\omega=75\ cm^{-1}$ is 160ps. Based on eq.9, the dephasing width is determined to be 15.5 cm^{-1}.

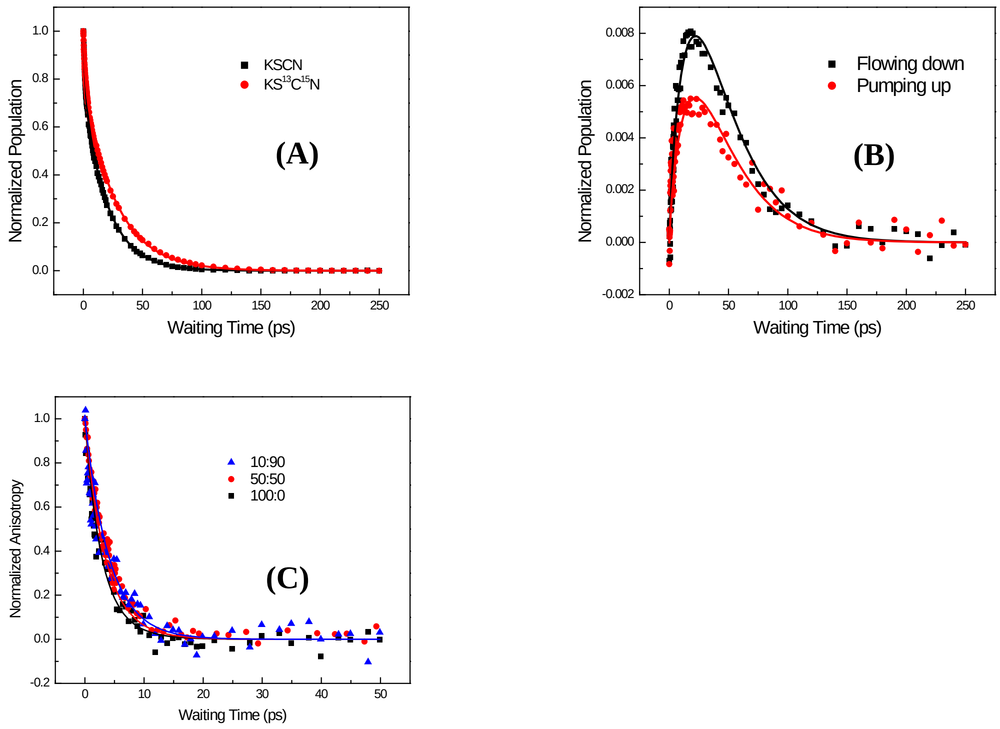

Figure S7. *Data and calculations of nonresonant [(A) and (B)] energy transfer between SCN^- and $S^{13}C^{15}N^-$ ($SCN^-/S^{13}C^{15}N^-$=1/1) and resonant [(C)] energy transfers among SCN^- anions for a 1.0M KSCN aqueous solution from our previous publication.*[1] *Dots are data, and lines are calculations. Calculations for (A) and (B) are with input parameters:*

$k_{SCN^- fast} = 1/1.7\ (ps^{-1})$; $k_{SCN^- slow} = 1/21\ (ps^{-1})$; $k_{S^{13}C^{15}N^- fast} = 1/1.6\ (ps^{-1})$; $k_{S^{13}C^{15}N^- slow} = 1/28\ (ps^{-1})$; $k_{clu \to iso} = 1/10\ (ps^{-1})$; K=0.38; $k_{SCN^- \to S^{13}C^{15}N^-} = 1/180\ (ps^{-1})$; D=0.70

with pre-factors of the subgroups and offset of the bi-exponential

$A_{SCN^- fast} = 0.25$; $A_{SCN^- slow} = 0.75$; $A_{S^{13}C^{15}N^- fast} = 0.21$; $A_{S^{13}C^{15}N^- slow} = 0.79$; $offset = 0$.

(C) $\tau_{or} = 4.3 ps$ *is experimentally determined, which is the rotation time of the clustered ions.* $n_{tot} = 3$, $\tau = 15 ps$. Therefore, for the same number of acceptors, the resonant transfer time is 15/1.5=10ps, and that for $\Delta\omega = 75\ cm^{-1}$ is 180ps. Based on eq.9, the dephasing width is determined to be 15.5 cm^{-1}.

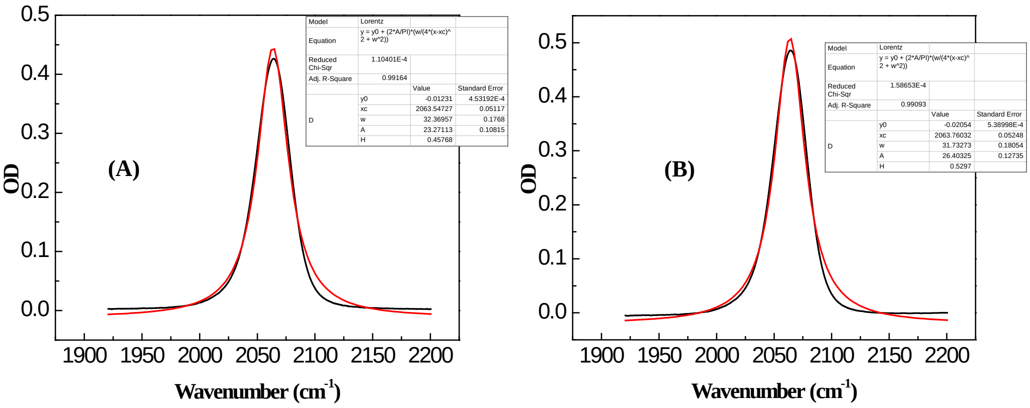

Figure S8. *FTIR spectra of 1M and 1.8M KSCN in D_2O solutions. The Lorentzian line width for both samples is 32 cm^{-1}, giving the dephasing width 16 cm^{-1}.*

Calculations of the transition dipole moment of the CN stretch in KSCN crystal

The transition dipole moment of the CN stretch was calculated by comparing the FTIR spectra and the 2D-IR signals for both of the CO stretch in the molecule $(CH_3C_5H_4)Mn(CO)_3$ and the CN stretch in KSCN crystal. Under the same experimental conditions, e.g. the pump intensity, the signal intensities can be expressed as:

$$I_{FTIR-CO} = C_1 \mu_{CO}^2 \quad \text{eq.S36}$$

$$I_{FTIR-CN} = C_1 \mu_{CN}^2 \quad \text{eq.S37}$$

$$I_{2DIR-CO} = C_2 \mu_{CO}^4 \quad \text{eq.S38}$$

$$I_{2DIR-CN} = C_2 \mu_{CN}^4 \ . \quad \text{eq.S39}$$

It is based the fact that, FTIR measurement is a linear spectroscopy, while 2D-IR method measures the 3rd order nonlinear response. From eq.S36-S39, we have

$$\frac{\mu_{CN}}{\mu_{CO}} = \sqrt{\frac{I_{2DIR-CN} / I_{2DIR-CO}}{I_{FTIR-CN} / I_{FTIR-CO}}} \ . \quad \text{eq.S40}$$

The transition dipole moment of the CO stretch was obtained by measuring the FTIR spectra of $(CH_3C_5H_4)Mn(CO)_3$ in CCl_4 solution with the concentration 0.029 M and the path length 25 μm (fig.S9A), and using the expression

$$\mu^2 = 9.186 \times 10^{-3} n \int [\varepsilon(\tilde{\nu}) / \tilde{\nu}] d\tilde{\nu} \ , \quad \text{eq.S41}$$

where μ is in the unit of Debye, $\tilde{\nu}$ is the wavenumber in cm^{-1}, $\varepsilon(\tilde{\nu})$ is the molar decadic extinction coefficient in L/(mol cm) at wavenumber $\tilde{\nu}$, and n is the refractive index of the media [11]. For CCl_4 solution at around 2022 cm^{-1}, $n = 1.44$. From the FTIR data and these parameters, we got $\mu_{CO} = 0.45D$.

The intensity ratios in eq. S40 were obtained from the FTIR and 2D-IR measurements for two samples. We got $I_{FTIR-CN} / I_{FTIR-CO} = 0.48 / 0.44$ (fig.S9A&B), and $I_{2DIR-CN} / I_{2DIR-CO} = 0.032 / 0.067$ for the intensity of red peak (fig.S10A&B) $I_{2DIR-CN} / I_{2DIR-CO} = 0.029 / 0.052$ for the intensity of blue peak (fig.S10C&D). By inserting all these ratios into eq.S40, we finally got the transition dipole moment of the CN stretch $\mu_{CN} = 0.30D$ (using red peak), or $\mu_{CN} = 0.32D$ (using blue peak). As a result, we chose $\mu_{CN} = 0.31D$ for the calculations in this work.

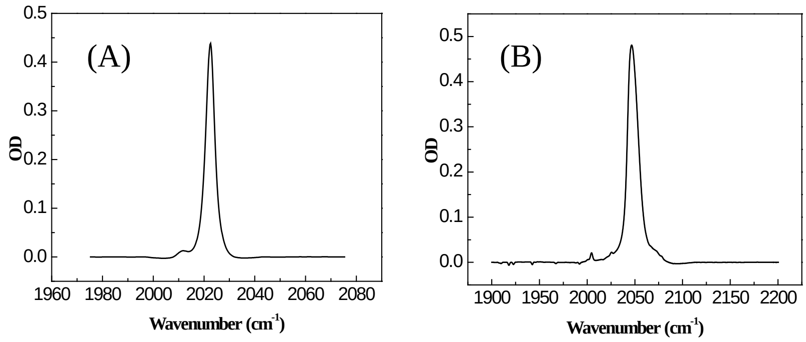

Figure S9. *FTIR spectra of (A) $(CH_3C_5H_4)Mn(CO)_3$ in CCl_4 solution with the concentration 0.029 M and the path length 25 μm, and (B) the thin film of polycrystalline KSCN crystals blended with ~50 wt% PMMA.*

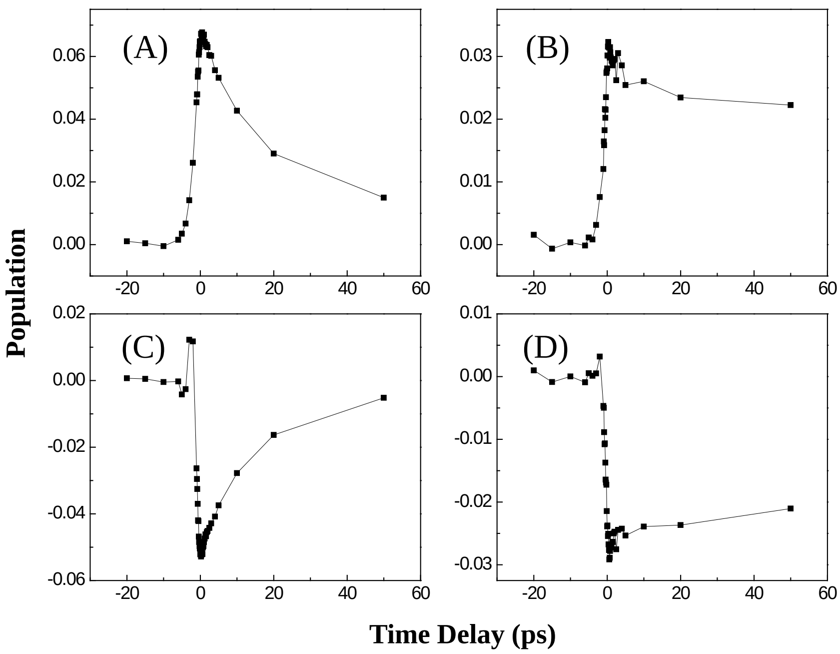

Figure S10. *Waiting time dependent intensities of the (A) red peak for $(CH_3C_5H_4)Mn(CO)_3$ solution, (B) red peak for KSCN crystal, (C) blue peak for $(CH_3C_5H_4)Mn(CO)_3$ solution, and (D) blue peak for KSCN crystal, all of which were measured by 2D-IR method, with the pump at 2022 cm^{-1} for the $(CH_3C_5H_4)Mn(CO)_3$ solution and 2050 cm^{-1} for the KSCN crystal.*

The derivation of the relation between the one-way energy transfer rate and the total energy transfer rate

For the energy transfer between a pair of donor and acceptor, without considering the vibrational relaxations, we have the rate equations

$$\frac{d}{dt}D(t) = -k_{DA}D(t) + k_{AD}A(t) \qquad \text{eq.S42}$$

$$\frac{d}{dt}A(t) = -k_{AD}A(t) + k_{DA}D(t)\,, \qquad \text{eq.S43}$$

where $D(t)$ and $A(t)$ are the populations of the exited state for the donor and acceptor, respectively, and k_{DA} (or k_{AD}) is the energy transfer rate from the donor (or acceptor) to the acceptor (or the donor). For both of the donor and the acceptor are identical SCN^- anions, we chose $k = k_{DA} + k_{AD}$ to denote the one-way energy transfer rate. Considering the initial conditions, $D(0) = 1$ and $A(0) = 0$. We get the solutions

$$D(t) = \frac{1}{2}e^{-kt} + \frac{1}{2} \qquad \text{eq.S44}$$

$$A(t) = -\frac{1}{2}e^{-kt} + \frac{1}{2}\,. \qquad \text{eq.S45}$$

Therefore, the total energy transfer rate is $k = k_{DA} + k_{AD}$, and $k_{DA} = e^{\frac{\Delta\omega_{DA}}{RT}} k_{AD}$.

Energy transfer dephasing time of the KSCN crystalline samples

The energy transfer dephasing time in eq.9 is a situation dependent parameter. If the dephasings of the donor and acceptor are uncorrelated, the energy transfer dephasing time (in terms of line width) is the convoluted line width of the donor and acceptor. For Lorentzian lineshapes, it is the sum of both donor and acceptor line widths, which determines the fastest value of possible energy transfer dephasing time. In many electronic energy transfers, such a dephasing time is assumed as the donor and the acceptor are several nm away so that it is reasonable to assume that the donor/acceptor dephasings are uncorrelated. For vibrational energy transfers, such an assumption may not be valid as the majority of experimentally measurable intermolecular vibrational energy transfers occur within distances smaller than 1 nm. Within such short distances, a molecular event which causes the dephasing of one molecule will inevitably affect the vibration of another molecule nearby. Therefore, the dephasings of the donor and the acceptor are correlated. The result of such a correlation is that the energy transfer dephasing time must be longer than that determined by the donor/acceptor convoluted line width. How long the energy transfer dephasing time can be is determined by how the dephasings of donor and acceptor are correlated. Experimentally, the energy transfer dephasing time can be obtained from the energy mismatch $\Delta\omega$ dependent energy transfers based on eq.9. In principle, if we know the energy transfer rate constants for two energy mismatches, mathematically we can derive the coupling strength and the dephasing time from eq.9. The condition for such a treatment is that the nonresonant energy transfer through the dephasing mechanism (eq.9) is much faster than that of the phonon compensation mechanism [12,13]. We expect that the condition can be fulfilled for most liquid solutions with relatively small energy mismatches ($\Delta\omega < RT$) where the dephasing is fast and well defined phonon motions are scarce. The condition can be invalid for some solid samples where the dephasing is relatively slow and the density of phonons with energy the same as the donor/acceptor mismatch is high.

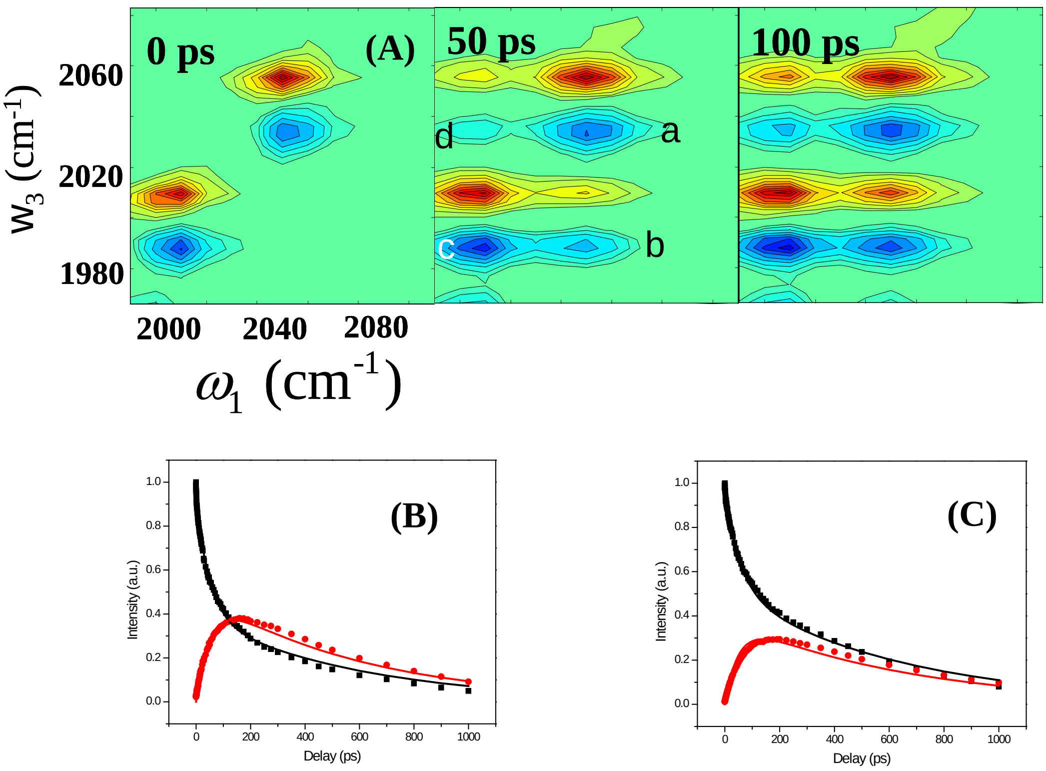

Figure S11. *(A):Waiting time dependent vibrational energy exchange 2D IR spectra of a KSCN/KS^{13}CN=1/1 mixed crystal at room temperature. The growth of cross peaks indicates how fast the vibrational energy exchange proceeds between SCN$^-$ and S^{13}CN$^-$. (B)-(C) Waiting time dependent normalized intensities of peaks a, b, c, and d. Dots are experimental data, and curves are calculations based on the energy exchange kinetic model and experimentally measured vibrational lifetimes.*Calculation parameters are *pfa=0.081; pfb=0.022; kfa=1/1.05; kfb=1/0.73; ka=1/589; kb=1/688; kab=1/96; and kba=1/123.*

The KSCN crystalline sample with a mismatch 75 cm^{-1} is such an example. As analyzed in the main text, in the KSCN/KS^{13}C^{15}N=1/1 sample, the energy transfer time constant ($\frac{1}{k}$) from SCN to S^{13}C^{15}N ($\Delta\omega = 75\ cm^{-1}$) is 99ps, and that from SCN to SCN ($\Delta\omega = 0\ cm^{-1}$) is 3.6ps. As shown in fig.S11, in the KSCN/KS^{13}CN=1/1 sample, the energy transfer time constant ($\frac{1}{k}$) from SCN to S^{13}CN ($\Delta\omega = 50\ cm^{-1}$) is 96ps. The results with three different energy mismatches cannot be described by eq.9 as it predicts that the energy transfer with $\Delta\omega = 50\ cm^{-1}$ should be 100% faster than that with $\Delta\omega = 75\ cm^{-1}$. The essential reason for the energy transfer from SCN to S^{13}C^{15}N is much faster than the prediction from eq.9 is that the measured energy transfer is from the phonon compensation mechanism. As we can see from both

Raman and Neutron scattering data, the phonon densities at ~ 75 cm^{-1} are much higher than those at around 50 cm^{-1}. Therefore, the energy transfer dephasing time can only be calculated from the results of samples with $\Delta\omega = 50\ cm^{-1}$ and $\Delta\omega = 0\ cm^{-1}$. Calculations show that the dephasing time is 8 cm^{-1} (in terms of line width), narrower than the convoluated line width (10 cm^{-1}). However, 8 cm^{-1} is only the fast limit of the dephasing time, as we don't know how much portion of the measured $\Delta\omega = 50\ cm^{-1}$ energy transfer is from the energy compensation mechanism. To test the uncertainty range of determined distance caused by this dephasing time uncertainty, we varied the dephasing time from 3 cm^{-1} to 8 cm^{-1}, and found that the calculated distance between two closest anions varies from 4.4 to 3.9 angstroms. The determined values are within experimental uncertainty (~10% of the actual distance 4 angstroms).

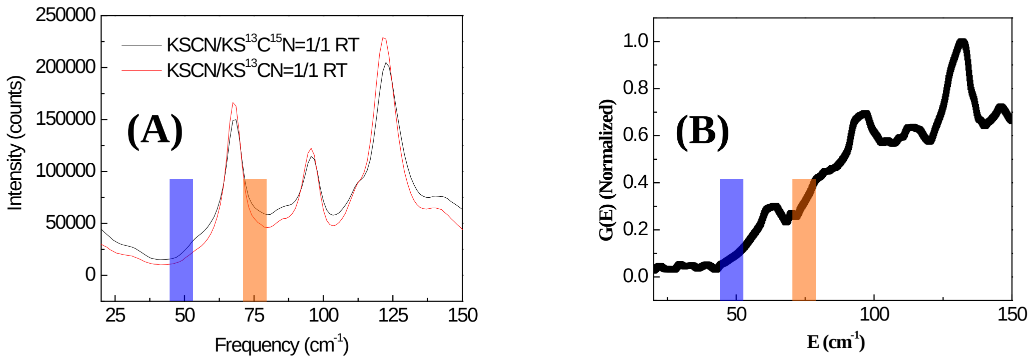

Figure S12. *(A) Raman spectra of KSCN/KS^{13}C^{15}N=1/1 and KSCN/KS^{13}CN=1/1 samples at room temperature; (B) Neutron scattering data at 10K from literature* [14].

Table of parameters of SCN^- in KSCN crystal

Table S2. Calculated parameters of every SCN^- in KSCN crystal (3*3*3, 500 anions). The orientation factors were calculated based on eq.S9, with $A_\infty = 0.7$. The coupling constants were calculated based on eq.10, with $n = 1.5$, $\mu_D = \mu_A = 0.31D$. Since the energy transfer rate for the donor to each of the acceptors is proportional to $\beta^2 / [(2\beta)^2 + \tau^{-2}]$ (see eq.9), the $1/k_{ET}$ for every SCN^- can be calculated by distributing the total energy transfer rate 1/1.8ps, which was obtained from experimental result, with $\tau^{-1} = 8\ cm^{-1}$.

No.	Distance (Å)	Orientation factor	Coupling constant (cm^{-1})	$1/k_{ET}$	No.	Distance (Å)	Orientation factor	Coupling constant (cm^{-1})	$1/k_{ET}$
0	0.000	0.000	0.000	0	1	4.017	0.378	1.252	29
2	4.017	0.378	1.252	29	3	4.026	0.706	2.324	8
4	4.026	0.706	2.324	8	5	4.802	0.477	0.926	53
6	4.802	0.477	0.926	53	7	5.576	0.597	0.740	82
8	5.576	0.597	0.740	82	9	6.160	0.740	0.681	97
10	6.160	0.740	0.681	97	11	6.451	0.728	0.583	133
12	6.451	0.728	0.583	133	13	6.532	0.950	0.732	84
14	6.532	0.950	0.732	84	15	6.673	0.626	0.452	220
16	6.673	0.626	0.452	220	17	6.715	0.672	0.477	198
18	6.715	0.672	0.477	198	19	7.517	1.182	0.598	126
20	7.517	1.182	0.598	126	21	7.543	0.899	0.450	222
22	7.543	0.899	0.450	222	23	7.789	0.991	0.451	222
24	7.789	0.991	0.451	222	25	7.789	0.991	0.451	222
26	7.789	0.991	0.451	222	27	8.550	0.385	0.132	2.57E+03
28	8.550	0.385	0.132	2.57E+03	29	8.550	0.385	0.132	2.57E+03
30	8.550	0.385	0.132	2.57E+03	31	8.932	1.139	0.343	3.82E+02
32	8.932	1.139	0.343	3.82E+02	33	9.338	0.523	0.138	2.37E+03
34	9.338	0.523	0.138	2.37E+03	35	9.338	0.523	0.138	2.37E+03
36	9.338	0.523	0.138	2.37E+03	37	9.380	0.417	0.109	3.82E+03
38	9.380	0.417	0.109	3.82E+0	39	9.380	0.417	0.109	3.82E+0

				3					3
40	9.380	0.417	0.109	3.82E+03	41	9.467	1.784	0.452	2.21E+02
42	9.467	1.784	0.452	2.21E+02	43	9.467	1.784	0.452	2.21E+02
44	9.467	1.784	0.452	2.21E+02	45	9.507	1.054	0.263	6.49E+02
46	9.507	1.054	0.263	6.49E+02	47	9.731	0.932	0.217	9.54E+02
48	9.731	0.932	0.217	9.54E+02	49	9.861	0.844	0.189	1.26E+03
50	9.861	0.844	0.189	1.26E+03	51	10.071	0.507	0.107	3.96E+03
52	10.071	0.507	0.107	3.96E+03	53	10.071	0.507	0.107	3.96E+03
54	10.071	0.507	0.107	3.96E+03	55	10.099	0.492	0.103	4.27E+03
56	10.099	0.492	0.103	4.27E+03	57	10.099	0.492	0.103	4.27E+03
58	10.099	0.492	0.103	4.27E+03	59	10.315	1.253	0.245	7.49E+02
60	10.315	1.253	0.245	7.49E+02	61	10.467	0.715	0.134	2.52E+03
62	10.467	0.715	0.134	2.52E+03	63	10.761	0.755	0.130	2.66E+03
64	10.761	0.755	0.130	2.66E+03	65	11.012	0.990	0.159	1.78E+03
66	11.012	0.990	0.159	1.78E+03	67	11.150	0.528	0.082	6.74E+03
68	11.150	0.528	0.082	6.74E+03	69	11.150	0.528	0.082	6.74E+03
70	11.150	0.528	0.082	6.74E+03	71	11.399	0.333	0.048	1.93E+04
72	11.399	0.333	0.048	1.93E+04	73	11.620	1.146	0.157	1.83E+03
74	11.620	1.146	0.157	1.83E+03	75	11.699	0.763	0.102	4.30E+03
76	11.699	0.763	0.102	4.30E+03	77	11.911	0.449	0.057	1.38E+04
78	11.911	0.449	0.057	1.38E+04	79	12.104	0.874	0.106	4.02E+03
80	12.104	0.874	0.106	4.02E+03	81	12.104	0.874	0.106	4.02E+03

82	12.104	0.874	0.106	4.02E+03	83	12.104	0.874	0.106	4.02E+03
84	12.104	0.874	0.106	4.02E+03	85	12.104	0.874	0.106	4.02E+03
86	12.104	0.874	0.106	4.02E+03	87	12.136	0.726	0.087	5.92E+03
88	12.136	0.726	0.087	5.92E+03	89	12.136	0.726	0.087	5.92E+03
90	12.136	0.726	0.087	5.92E+03	91	12.262	0.446	0.052	1.67E+04
92	12.262	0.446	0.052	1.67E+04	93	12.318	0.858	0.099	4.63E+03
94	12.318	0.858	0.099	4.63E+03	95	12.467	0.852	0.095	5.05E+03
96	12.467	0.852	0.095	5.05E+03	97	12.508	0.424	0.047	2.08E+04
98	12.508	0.424	0.047	2.08E+04	99	12.625	1.249	0.133	2.53E+03
100	12.625	1.249	0.133	2.53E+03	101	12.667	1.248	0.132	2.59E+03
102	12.667	1.248	0.132	2.59E+03	103	12.778	0.866	0.089	5.67E+03
104	12.778	0.866	0.089	5.67E+03	105	12.778	0.866	0.089	5.67E+03
106	12.778	0.866	0.089	5.67E+03	107	12.855	1.242	0.126	2.85E+03
108	12.855	1.242	0.126	2.85E+03	109	12.995	1.579	0.155	1.89E+03
110	12.995	1.579	0.155	1.89E+03	111	13.050	0.472	0.046	2.17E+04
112	13.050	0.472	0.046	2.17E+04	113	13.208	0.496	0.046	2.10E+04
114	13.208	0.496	0.046	2.10E+04	115	13.208	0.496	0.046	2.10E+04
116	13.208	0.496	0.046	2.10E+04	117	13.346	0.626	0.057	1.41E+04
118	13.346	0.626	0.057	1.41E+04	119	13.348	0.731	0.066	1.03E+04
120	13.348	0.731	0.066	1.03E+04	121	13.348	0.731	0.066	1.03E+04
122	13.348	0.731	0.066	1.03E+04	123	13.430	0.672	0.060	1.27E+04
124	13.430	0.672	0.060	1.27E+04	125	13.438	0.523	0.046	2.10E+04

126	13.438	0.523	0.046	2.10E+04	127	13.854	0.862	0.070	9.30E+03
128	13.854	0.862	0.070	9.30E+03	129	13.854	0.862	0.070	9.30E+03
130	13.854	0.862	0.070	9.30E+03	131	13.913	0.573	0.046	2.16E+04
132	13.913	0.573	0.046	2.16E+04	133	13.937	1.229	0.098	4.74E+03
134	13.937	1.229	0.098	4.74E+03	135	13.937	1.229	0.098	4.74E+03
136	13.937	1.229	0.098	4.74E+03	137	14.177	0.413	0.031	4.65E+04
138	14.177	0.413	0.031	4.65E+04	139	14.177	0.413	0.031	4.65E+04
140	14.177	0.413	0.031	4.65E+04	141	14.280	0.795	0.059	1.31E+04
142	14.280	0.795	0.059	1.31E+04	143	14.280	0.795	0.059	1.31E+04
144	14.280	0.795	0.059	1.31E+04	145	14.439	0.447	0.032	4.42E+04
146	14.439	0.447	0.032	4.42E+04	147	14.527	0.453	0.032	4.47E+04
148	14.527	0.453	0.032	4.47E+04	149	14.612	0.875	0.060	1.24E+04
150	14.612	0.875	0.060	1.24E+04	151	14.859	0.971	0.064	1.11E+04
152	14.859	0.971	0.064	1.11E+04	153	14.859	0.971	0.064	1.11E+04
154	14.859	0.971	0.064	1.11E+04	155	14.940	1.527	0.098	4.66E+03
156	14.940	1.527	0.098	4.66E+03	157	14.940	1.527	0.098	4.66E+03
158	14.940	1.527	0.098	4.66E+03	159	14.945	0.806	0.052	1.67E+04
160	14.945	0.806	0.052	1.67E+04	161	14.985	0.861	0.055	1.49E+04
162	14.985	0.861	0.055	1.49E+04	163	14.996	1.556	0.099	4.59E+03
164	14.996	1.556	0.099	4.59E+03	165	14.996	1.556	0.099	4.59E+03
166	14.996	1.556	0.099	4.59E+03	167	15.007	0.508	0.032	4.32E+04
168	15.007	0.508	0.032	4.32E+04	169	15.086	0.899	0.056	1.42E+04

170	15.086	0.899	0.056	1.42E+04	171	15.152	0.825	0.051	1.74E+04
172	15.152	0.825	0.051	1.74E+04	173	15.285	1.285	0.077	7.55E+03
174	15.285	1.285	0.077	7.55E+03	175	15.330	0.467	0.028	5.81E+04
176	15.330	0.467	0.028	5.81E+04	177	15.330	0.467	0.028	5.81E+04
178	15.330	0.467	0.028	5.81E+04	179	15.403	0.485	0.029	5.54E+04
180	15.403	0.485	0.029	5.54E+04	181	15.403	0.485	0.029	5.54E+04
182	15.403	0.485	0.029	5.54E+04	183	15.410	0.477	0.028	5.74E+04
184	15.410	0.477	0.028	5.74E+04	185	15.410	0.477	0.028	5.74E+04
186	15.410	0.477	0.028	5.74E+04	187	15.431	0.428	0.025	7.19E+04
188	15.431	0.428	0.025	7.19E+04	189	15.431	0.428	0.025	7.19E+04
190	15.431	0.428	0.025	7.19E+04	191	15.614	0.344	0.019	1.20E+05
192	15.614	0.344	0.019	1.20E+05	193	15.614	0.344	0.019	1.20E+05
194	15.614	0.344	0.019	1.20E+05	195	15.990	0.588	0.031	4.72E+04
196	15.990	0.588	0.031	4.72E+04	197	16.015	0.886	0.046	2.10E+04
198	16.015	0.886	0.046	2.10E+04	199	16.059	0.726	0.038	3.18E+04
200	16.059	0.726	0.038	3.18E+04	201	16.059	0.726	0.038	3.18E+04
202	16.059	0.726	0.038	3.18E+04	203	16.083	0.359	0.019	1.31E+05
204	16.083	0.359	0.019	1.31E+05	205	16.083	0.359	0.019	1.31E+05
206	16.083	0.359	0.019	1.31E+05	207	16.253	0.573	0.029	5.49E+04
208	16.253	0.573	0.029	5.49E+04	209	16.407	1.656	0.081	6.95E+03
210	16.407	1.656	0.081	6.95E+03	211	16.473	0.488	0.023	8.21E+04
212	16.473	0.488	0.023	8.21E+04	213	16.496	0.732	0.035	3.67E+04

214	16.496	0.732	0.035	3.67E+04	215	16.496	0.732	0.035	3.67E+04
216	16.496	0.732	0.035	3.67E+04	217	16.513	0.722	0.034	3.80E+04
218	16.513	0.722	0.034	3.80E+04	219	16.513	0.722	0.034	3.80E+04
220	16.513	0.722	0.034	3.80E+04	221	16.528	0.789	0.038	3.20E+04
222	16.528	0.789	0.038	3.20E+04	223	16.560	0.570	0.027	6.20E+04
224	16.560	0.570	0.027	6.20E+04	225	16.678	0.937	0.043	2.40E+04
226	16.678	0.937	0.043	2.40E+04	227	16.678	0.937	0.043	2.40E+04
228	16.678	0.937	0.043	2.40E+04	229	16.704	0.577	0.027	6.38E+04
230	16.704	0.577	0.027	6.38E+04	231	16.736	1.099	0.050	1.78E+04
232	16.736	1.099	0.050	1.78E+04	233	16.736	1.099	0.050	1.78E+04
234	16.736	1.099	0.050	1.78E+04	235	16.736	1.099	0.050	1.78E+04
236	16.736	1.099	0.050	1.78E+04	237	16.736	1.099	0.050	1.78E+04
238	16.736	1.099	0.050	1.78E+04	239	16.787	1.124	0.051	1.73E+04
240	16.787	1.124	0.051	1.73E+04	241	16.787	1.124	0.051	1.73E+04
242	16.787	1.124	0.051	1.73E+04	243	16.787	1.124	0.051	1.73E+04
244	16.787	1.124	0.051	1.73E+04	245	16.787	1.124	0.051	1.73E+04
246	16.787	1.124	0.051	1.73E+04	247	16.796	0.476	0.022	9.67E+04
248	16.796	0.476	0.022	9.67E+04	249	16.796	0.476	0.022	9.67E+04
250	16.796	0.476	0.022	9.67E+04	251	16.812	0.738	0.033	4.04E+04
252	16.812	0.738	0.033	4.04E+04	253	16.934	1.320	0.058	1.32E+04
254	17.368	1.208	0.050	1.84E+04	255	17.551	0.840	0.033	4.04E+04
256	17.551	0.840	0.033	4.04E+04	257	17.551	0.840	0.033	4.04E+04

258	17.551	0.840	0.033	4.04E+04	259	17.810	0.450	0.017	1.54E+05
260	17.810	0.450	0.017	1.54E+05	261	17.810	0.450	0.017	1.54E+05
262	17.810	0.450	0.017	1.54E+05	263	17.810	0.450	0.017	1.54E+05
264	17.810	0.450	0.017	1.54E+05	265	17.810	0.450	0.017	1.54E+05
266	17.810	0.450	0.017	1.54E+05	267	17.824	0.590	0.022	9.00E+04
268	17.824	0.590	0.022	9.00E+04	269	17.824	0.590	0.022	9.00E+04
270	17.824	0.590	0.022	9.00E+04	271	17.832	0.475	0.018	1.39E+05
272	17.832	0.475	0.018	1.39E+05	273	17.832	0.475	0.018	1.39E+05
274	17.832	0.475	0.018	1.39E+05	275	18.091	0.884	0.032	4.39E+04
276	18.091	0.884	0.032	4.39E+04	277	18.111	1.258	0.046	2.18E+04
278	18.111	1.258	0.046	2.18E+04	279	18.184	1.539	0.055	1.49E+04
280	18.184	1.539	0.055	1.49E+04	281	18.275	0.526	0.019	1.31E+05
282	18.275	0.526	0.019	1.31E+05	283	18.275	0.526	0.019	1.31E+05
284	18.275	0.526	0.019	1.31E+05	285	18.291	0.713	0.025	7.19E+04
286	18.291	0.713	0.025	7.19E+04	287	18.291	0.713	0.025	7.19E+04
288	18.291	0.713	0.025	7.19E+04	289	18.300	0.462	0.016	1.72E+05
290	18.300	0.462	0.016	1.72E+05	291	18.371	0.502	0.017	1.49E+05
292	18.371	0.502	0.017	1.49E+05	293	18.371	0.502	0.017	1.49E+05
294	18.371	0.502	0.017	1.49E+05	295	18.394	0.874	0.030	4.95E+04
296	18.394	0.874	0.030	4.95E+04	297	18.538	1.122	0.038	3.15E+04
298	18.538	1.122	0.038	3.15E+04	299	18.639	0.908	0.030	4.97E+04
300	18.639	0.908	0.030	4.97E+04	301	18.678	0.487	0.016	1.75E+05

302	18.678	0.487	0.016	1.75E+05	303	18.678	0.487	0.016	1.75E+05
304	18.678	0.487	0.016	1.75E+05	305	18.800	1.089	0.035	3.63E+04
306	18.800	1.089	0.035	3.63E+04	307	18.908	0.331	0.011	4.06E+05
308	18.934	1.784	0.056	1.41E+04	309	18.934	1.784	0.056	1.41E+04
310	18.934	1.784	0.056	1.41E+04	311	18.934	1.784	0.056	1.41E+04
312	18.935	1.038	0.033	4.18E+04	313	18.935	1.038	0.033	4.18E+04
314	18.998	0.871	0.027	6.05E+04	315	19.042	0.564	0.018	1.47E+05
316	19.042	0.564	0.018	1.47E+05	317	19.042	0.564	0.018	1.47E+05
318	19.042	0.564	0.018	1.47E+05	319	19.090	0.847	0.026	6.59E+04
320	19.243	0.531	0.016	1.76E+05	321	19.243	0.531	0.016	1.76E+05
322	19.279	0.585	0.018	1.47E+05	323	19.279	0.585	0.018	1.47E+05
324	19.279	0.585	0.018	1.47E+05	325	19.279	0.585	0.018	1.47E+05
326	19.373	0.838	0.025	7.35E+04	327	19.373	0.838	0.025	7.35E+04
328	19.476	0.883	0.026	6.84E+04	329	19.570	0.993	0.028	5.56E+04
330	19.570	0.993	0.028	5.56E+04	331	19.570	0.880	0.025	7.08E+04
332	19.597	0.353	0.010	4.43E+05	333	19.619	1.097	0.031	4.63E+04
334	19.619	1.097	0.031	4.63E+04	335	19.619	1.097	0.031	4.63E+04
336	19.619	1.097	0.031	4.63E+04	337	19.626	0.580	0.016	1.66E+05
338	19.626	0.580	0.016	1.66E+05	339	19.797	0.718	0.020	1.14E+05
340	19.797	0.718	0.020	1.14E+05	341	19.797	0.718	0.020	1.14E+05
342	19.797	0.718	0.020	1.14E+05	343	19.947	0.680	0.018	1.33E+05
344	20.051	0.383	0.010	4.32E+05	345	20.051	0.383	0.010	4.32E+05

346	20.139	0.705	0.019	1.31E+05	347	20.142	0.507	0.013	2.54E+05
348	20.142	0.507	0.013	2.54E+05	349	20.142	0.507	0.013	2.54E+05
350	20.142	0.507	0.013	2.54E+05	351	20.162	0.703	0.018	1.33E+05
352	20.162	0.703	0.018	1.33E+05	353	20.198	0.492	0.013	2.73E+05
354	20.198	0.492	0.013	2.73E+05	355	20.198	0.492	0.013	2.73E+05
356	20.198	0.492	0.013	2.73E+05	357	20.203	0.416	0.011	3.83E+05
358	20.203	0.416	0.011	3.83E+05	359	20.203	0.416	0.011	3.83E+05
360	20.203	0.416	0.011	3.83E+05	361	20.291	0.509	0.013	2.63E+05
362	20.291	0.509	0.013	2.63E+05	363	20.291	0.509	0.013	2.63E+05
364	20.291	0.509	0.013	2.63E+05	365	20.381	0.899	0.023	8.66E+04
366	20.381	0.899	0.023	8.66E+04	367	20.381	0.899	0.023	8.66E+04
368	20.381	0.899	0.023	8.66E+04	369	20.381	1.453	0.037	3.31E+04
370	20.381	1.453	0.037	3.31E+04	371	20.381	1.453	0.037	3.31E+04
372	20.381	1.453	0.037	3.31E+04	373	20.441	0.779	0.020	1.17E+05
374	20.441	0.779	0.020	1.17E+05	375	20.450	0.805	0.020	1.10E+05
376	20.450	0.805	0.020	1.10E+05	377	20.522	0.403	0.010	4.48E+05
378	20.702	0.369	0.009	5.65E+05	379	20.702	0.369	0.009	5.65E+05
380	20.882	0.621	0.015	2.10E+05	381	20.943	0.632	0.015	2.06E+05
382	21.082	1.000	0.023	8.57E+04	383	21.082	1.000	0.023	8.57E+04
384	21.182	0.456	0.010	4.24E+05	385	21.182	0.456	0.010	4.24E+05
386	21.232	0.552	0.012	2.93E+05	387	21.232	0.552	0.012	2.93E+05
388	21.232	0.552	0.012	2.93E+05	389	21.232	0.552	0.012	2.93E+05

390	21.232	0.552	0.012	2.93E+05	391	21.232	0.552	0.012	2.93E+05
392	21.232	0.552	0.012	2.93E+05	393	21.232	0.552	0.012	2.93E+05
394	21.236	0.853	0.019	1.23E+05	395	21.244	0.463	0.010	4.18E+05
396	21.244	0.463	0.010	4.18E+05	397	21.244	0.463	0.010	4.18E+05
398	21.244	0.463	0.010	4.18E+05	399	21.272	0.564	0.013	2.84E+05
400	21.272	0.564	0.013	2.84E+05	401	21.272	0.564	0.013	2.84E+05
402	21.272	0.564	0.013	2.84E+05	403	21.272	0.564	0.013	2.84E+05
404	21.272	0.564	0.013	2.84E+05	405	21.272	0.564	0.013	2.84E+05
406	21.272	0.564	0.013	2.84E+05	407	21.279	0.426	0.009	5.00E+05
408	21.279	0.426	0.009	5.00E+05	409	21.279	0.426	0.009	5.00E+05
410	21.279	0.426	0.009	5.00E+05	411	21.382	0.862	0.019	1.26E+05
412	21.498	1.591	0.034	3.81E+04	413	21.498	1.591	0.034	3.81E+04
414	21.505	0.648	0.014	2.30E+05	415	21.505	0.648	0.014	2.30E+05
416	21.580	0.378	0.008	6.89E+05	417	21.580	0.378	0.008	6.89E+05
418	21.616	0.716	0.015	1.94E+05	419	21.616	0.716	0.015	1.94E+05
420	21.797	0.737	0.015	1.93E+05	421	21.797	0.737	0.015	1.93E+05
422	21.797	0.737	0.015	1.93E+05	423	21.797	0.737	0.015	1.93E+05
424	21.983	0.725	0.015	2.10E+05	425	22.116	0.852	0.017	1.57E+05
426	22.116	0.852	0.017	1.57E+05	427	22.175	0.712	0.014	2.29E+05
428	22.378	0.523	0.010	4.49E+05	429	22.401	0.472	0.009	5.55E+05
430	22.508	0.468	0.009	5.80E+05	431	22.589	0.444	0.008	6.57E+05
432	22.679	0.799	0.015	2.08E+05	433	22.679	0.799	0.015	2.08E+05

434	22.810	0.744	0.013	2.49E+05	435	22.810	0.744	0.013	2.49E+05
436	22.924	0.472	0.008	6.36E+05	437	22.924	0.472	0.008	6.36E+05
438	22.924	0.472	0.008	6.36E+05	439	22.924	0.472	0.008	6.36E+05
440	23.005	0.755	0.013	2.54E+05	441	23.005	0.755	0.013	2.54E+05
442	23.144	0.577	0.010	4.51E+05	443	23.144	0.577	0.010	4.51E+05
444	23.351	0.454	0.008	7.68E+05	445	23.351	0.454	0.008	7.68E+05
446	23.556	0.890	0.015	2.11E+05	447	23.571	0.817	0.013	2.51E+05
448	23.571	0.817	0.013	2.51E+05	449	23.571	0.817	0.013	2.51E+05
450	23.571	0.817	0.013	2.51E+05	451	23.710	0.526	0.008	6.28E+05
452	23.710	0.526	0.008	6.28E+05	453	23.789	0.884	0.014	2.26E+05
454	23.839	0.892	0.014	2.25E+05	455	23.839	0.892	0.014	2.25E+05
456	23.979	0.619	0.010	4.85E+05	457	23.999	1.160	0.018	1.39E+05
458	23.999	1.160	0.018	1.39E+05	459	24.209	0.899	0.014	2.43E+05
460	24.209	0.899	0.014	2.43E+05	461	24.209	0.899	0.014	2.43E+05
462	24.209	0.899	0.014	2.43E+05	463	24.209	0.874	0.013	2.57E+05
464	24.209	0.874	0.013	2.57E+05	465	24.209	0.874	0.013	2.57E+05
466	24.209	0.874	0.013	2.57E+05	467	24.259	0.616	0.009	5.25E+05
468	24.259	0.616	0.009	5.25E+05	469	24.451	0.459	0.007	9.90E+05
470	24.466	0.499	0.007	8.40E+05	471	24.480	0.473	0.007	9.41E+05
472	24.480	0.473	0.007	9.41E+05	473	24.710	0.517	0.007	8.30E+05
474	24.754	0.688	0.010	4.75E+05	475	24.890	0.537	0.007	8.06E+05
476	24.890	0.537	0.007	8.06E+05	477	25.163	0.543	0.007	8.41E+05

478	25.163	0.543	0.007	8.41E+05	479	25.413	0.610	0.008	7.07E+05
480	25.413	0.610	0.008	7.07E+05	481	25.413	0.610	0.008	7.07E+05
482	25.413	0.610	0.008	7.07E+05	483	25.602	0.487	0.006	1.16E+06
484	25.602	0.487	0.006	1.16E+06	485	25.924	0.552	0.007	9.74E+05
486	26.005	0.554	0.007	9.82E+05	487	26.055	0.422	0.005	1.71E+06
488	26.055	0.422	0.005	1.71E+06	489	26.117	0.893	0.011	3.89E+05
490	26.117	0.893	0.011	3.89E+05	491	26.359	0.460	0.005	1.55E+06
492	26.771	0.867	0.010	4.78E+05	493	27.347	0.790	0.008	6.55E+05
494	27.443	0.431	0.004	2.25E+06	495	27.443	0.431	0.004	2.25E+06
496	28.347	0.704	0.007	1.02E+06	497	28.743	0.459	0.004	2.62E+06
498	28.743	0.459	0.004	2.62E+06	499	30.161	0.895	0.007	9.18E+05

Reference and Notes:

(1) Bian, H. T.; Wen, X. W.; Li, J. B.; Chen, H. L.; Han, S. Z.; Sun, X. Q.; Song, J. A.; Zhuang, W.; Zheng, J. R. Ion Clustering in Aqueous Solutions Probed with Vibrational Energy Transfer. *Proc. Natl. Acad. Sci. U. S. A.* **2011**, *108*, 4737-4742.

(2) Lipari, G.; Szabo, A. Effect of Librational Motion on Fluorescence Depolarization and Nuclear Magnietic Resonance Relaxation in Macromolecules and Membranes. *Biophys. J.* **1980**, *30*, 489-506.

(3) Kinosita Jr, K.; Kawato, S.; Ikegami, A. A Theory of Fluorescence Polarization Decay in Membranes. *Biophysical journal* **1977**, *20*, 289-305.

(4) Soleillet, P. Sur Les Parametres Caracterisant La Polarisation Partielle De La Lumiere Dans Les Phenomenes De Fluorescence. *Ann. Phys.* **1929**, *12*, 23-97.

(5) Dale, R. E.; Eisinger, J.; Blumberg, W. The Orientational Freedom of Molecular Probes. The Orientation Factor in Intramolecular Energy Transfer. *Biophys. J.* **1979**, *26*, 161-193.

(6) Li, J. B.; Bian, H. T.; Chen, H. L.; Hoang, B.; Zheng, J. R. Ion Association in Aqueous Solutions Probed through Vibrational Energy Transfers among Cation, Anion and Water Molecules. *J. Phys. Chem. B.* **2012**, *117*, 4274-4283.

(7) Chang, J. C. Monopole Effects on Electronic Excitation Interactions between Large Molecules. I. Application to Energy Transfer in Chlorophylls. *The Journal of*

chemical physics **1977**, *67*, 3901.

(8) Baumann, J.; Fayer, M. Excitation Transfer in Disordered Two-Dimensional and Anisotropic Three-Dimensional Systems: Effects of Spatial Geometry on Time-Resolved Observables. *The Journal of Chemical Physics* **1986**, *85*, 4087.

(9) Yang, M.; Li, F.; Skinner, J. Vibrational Energy Transfer and Anisotropy Decay in Liquid Water: Is the Förster Model Valid? *The Journal of Chemical Physics* **2011**, *135*, 164505.

(10) Bian, H. T.; Chen, H. L.; Li, J. B.; Wen, X. W.; Zheng, J. R. Nonresonant and Resonant Mode-Specific Intermolecular Vibrational Energy Transfers in Electrolyte Aqueous Solutions. *J. Phys. Chem. A.* **2011**, *115*, 11657-11664.

(11) Knox, R. S.; van Amerongen, H. Refractive Index Dependence of the Forster Resonance Excitation Transfer Rate. *J. Phys. Chem. B* **2002**, *106*, 5289-5293.

(12) Holstein, T.; Lyo, S.; Orbach, R. Phonon-Assisted Radiative Transfer. *Physical Review B* **1977**, *16*, 934.

(13) Holstein, T.; Lyo, S.; Orbach, R. Excitation Transfer in Disordered Systems. In *Laser Spectroscopy of Solids*; Springer: New York, 1986; pp 39-82.

(14) Natkaniec, I.; Smirnov, L.; Solov'ev, A. Ammonium Dynamics in the Ordered and Disordered Phases of $K_{1-x}(NH_4)_xSCN$ Solid Solutions. *Physica B: Condensed Matter* **1995**, *213*, 667-668.